Characteristics of radio-cesium transport and discharge between different basins near to the Fukushima Dai-ichi Nuclear Power Plant after heavy rainfall events

Kazuyuki Sakuma, [*1] Akihiro Kitamura, [1, 2] Alex Malins, [2] Hiroshi Kurikami, [1, 2] Masahiko Machida, [2] Koji Mori, [3] Kazuhiro Tada, [3] Takamaru Kobayashi, [3] Yasuhiro Tawara, [3] Hiroyuki Tosaka. [3]

[1] Sector of Fukushima Research and Development, Japan Atomic Energy Agency, 10-2 Fukasaku, Miharu-machi, Fukushima 963-7700, Japan,
[2] Center for Computational Science & e-Systems, Japan Atomic Energy Agency, University of Tokyo Kashiwanoha Campus Satellite, 178-4-4 Wakashiba, Kashiwa-shi, Chiba 277-0871, Japan,
[3] Geosphere Environmental Technology Corporation, 2-1 Kanda-Awajicho, Chiyoda-ku, Tokyo 101-0063, Japan,

[*]Corresponding author. E-mail address: sakuma.kazuyuki@jaea.go.jp (K. Sakuma)

Abstract

This paper describes watershed modeling of catchments surrounding the Fukushima Dai-ichi Nuclear Power Plant to understand radio-cesium redistribution by water flows and sediment transport. We extended our previously developed three-dimensional hydrogeological model of the catchments to calculate the migration of radio-cesium in both sediment-sorbed and dissolved forms. The simulations cover the entirety of 2013, including nine heavy rainfall events, as well as Typhoon Roke in September 2011. Typhoons Man-yi and Wipha were the strongest typhoons in 2013 and had the largest bearing on radio-cesium redistribution. The simulated ^{137}Cs discharge quantities over the nine events in 2013 are in good agreement with field monitoring observations. Deposition mainly occurs on flood plains and points where the river beds broaden in the lower basins, and within dam reservoirs along the rivers. Differences in ^{137}Cs discharge ratios between the five basins are explained by differences in the initial fallout distribution within the basins, the presence of dam reservoirs, and the input supply to watercourses. It is possible to use these simulation results to evaluate future radioactive material distributions in order to support remediation planning.

Key words: Fukushima Dai-ichi accident, radioactive cesium, sediment transport, watershed model

- Reports watershed modeling and ^{137}Cs transport calculations in eastern Fukushima.
- Results cover Odaka, Ukedo, Maeda, Kuma and Tomioka River basins surrounding Fukushima Dai-ichi.
- Simulations are of 2011 Typhoon Roke and nine rainfall events over 2013.
- Gives reasons for differences in discharge amounts between the different basins.
- Reports datasets of water, sediment and ^{137}Cs discharge to the Pacific Ocean over the events.

1. Introduction

The magnitude 9.0 earthquake and subsequent tsunami on 11 March 2011 instigated the Fukushima Dai-ichi Nuclear Power Plant (FDNPP) accident followed by the release of radionuclides into the environment (Katata et al., 2012; Terada et al., 2012; Kobayashi et al., 2013; Buesseler, 2014). Substantial endeavors have been paid to monitoring the distribution and fate of the radionuclides in the environment in order to comprehend human exposures to radiation and the effects on agriculture, forests, rivers and oceans in the region (Chartin et al., 2013; Gonze et al., 2014; Saito et al., 2014; Yoshimura et al., 2014; Takahashi et al., 2015).

Radioactive material was deposited on a wide range of land types after the accident. Based on learning after the Chernobyl accident, Onishi et al. (2007) recommended predicting contamination migration in the environment using simulations to assist in the design of countermeasures. In particular they recommended simulating the transport of radionuclides both dissolved in surface water flows and via transport in the soil-sorbed form by erosion and sediment redistribution. The results can then input into considerations for remediation and recovery, decisions to resume agricultural activities and reutilize irrigation systems, and for radiation protection purposes.

Previously some watershed scale simulations of soil erosion, sediment movement, and radio-cesium migration in Fukushima Prefecture were reported (Yamaguchi et al. (2014); Kitamura et al. (2014); Kinouchi et al. (2015); Mori et al., (2015)). Yamaguchi et al. (2014) and Kitamura et al. (2014) calculated soil loss and ^{137}Cs discharge for 14 river basins in eastern Fukushima using an empirical model, the Soil And Cesium Transport (SACT) model, which can cover broad areas (5432 km^2 in Kitamura et al.; 2014). Kinouchi et al. (2015) simulated the Kuchibuto River catchment (140 km^2) using a physically-based distributed hydrological and sediment erosion model, and Mori et al. (2015) studied the 15 km^2 Hokkawa Dam catchment using integrated watershed modeling.

Two complementary modeling approaches for watersheds include using simple, empirical models with minimal parameters to describe the data, or employing complex approaches capturing the underlying physical processes of the watershed. A risk of the former approach is that the model may lack sufficient complexity to describe the watershed dynamics, and physical interpretation of empirically fitted parameters can be difficult (Abbott et al., 1986). An issue with the latter however is that over-parameterization can lead to equifinality, creating uncertainty in the results (Beven, 1989). Our approach to these issues in our studies of Fukushima basins has been to employ both empirical (Kitamura et al., 2014) and physics-based models (Kitamura et al., 2016), coupled with targeted field monitoring (Saegusa et al., 2016), to deduce the dynamics of radio-cesium redistribution within the basins.

We previously developed a 3D model for five basins surrounding FDNPP in order to simulate water and sediment transport using a complex physics-based watershed simulation code (Kitamura et al., 2016). The five catchments studied comprise of forest, farmland and surface water systems such as rivers, lakes, dam reservoirs and ground water systems. In this paper we extend our previous study to calculate quantities of radio-cesium migration.

The key features of this study are that it covers five of the most highly contaminated catchments in terms of radio-cesium deposition density in Fukushima Prefecture. The catchments surround FDNPP and total 674 km^2 in area. We employed a fine resolution simulation mesh to determine the local areas with high radio-cesium accumulation. By considering five basins together, we could contrast each basin to determine the important factors controlling radio-cesium redistribution within each basin. The main results are datasets of cesium discharge information for each basin under floods with varying intensity. The datasets could be used to evaluate future radioactive cesium distributions, re-evaluate of the amount of radio-cesium dispersed and deposited on the land surface following the FDNPP accident, or to provide boundary conditions for more detailed river simulations or ocean models.

2. 3D hydrogeological structure model

The simulations are conducted on a 3D hydrogeological model of the study area, which covers the Odaka, Ukedo, Maeda, Kuma and Tomioka River basins (Kitamura et al., 2016; Fig. 1). The dominant land uses in the area are forests, rice paddies, crop fields and buildings, covering 60%, 22%, 7%, and 5% of the area, respectively. The physical characteristics, land use and ^{137}Cs contamination level of each basin are summarized in Table 1. The Ukedo basin consists two main rivers, the Ukedo and the Takase, and a large dam reservoir, the Ogaki Dam, which lies 22 km upstream of the Ukedo River mouth.

The model divides the region using a 3D mesh into different grid-blocks. Water, sediment and radio-cesium flows are evaluated between the different blocks in the model. The spacing of the mesh varies to account for topographical features. The mesh takes a fine structure around rivers and their neighboring grid regions, which are important areas to resolve sediment and fluid transport. The mesh is coarser over the forests, and locations far from rivers, for computational efficiency. The horizontal resolution of the mesh cells varies between 10-250 m (average 70 m). The mesh structure is shown in Fig. 2.

The ground was discretized into 28 layers of varying thickness to account for variations between geological strata of the subsurface. At ground level three surface soil layers can be eroded by rainfall impact or surface water flows, or added to by sediment deposition. The upper surface soil layer is 2 cm thick, with a 10 cm layer followed by an 18 cm layer beneath. In the initial state of the simulation all of the radio-cesium inventory is spread homogenously within the top 2 cm surface soil layer. This represents a reasonable approximation to the true depth distribution of radio-cesium within soil, which is typically exponential (Matsuda et al., 2015) with around 60~95% of the inventory within 2 cm from the surface.

Overland water flows occur in a layer termed the surface layer, which lies above the top surface soil layer. Eroded sediment is transported suspended within the overland flows in the surface layer. Likewise radio-cesium is transported within the surface layer in both the sediment-sorbed and dissolved forms. An air layer above tops the model. The total number of grid-blocks created was

4,224,000.

The hydrogeological structure of the 3D grid-block system (geology/deposit type, etc.) was assigned based on geological maps produced by the Geological Survey of Japan (2012) (see Kitamura et al., 2016). These data were used to initiate various parameters in the model, such as bedrock effective porosity and intrinsic permeability (Supplementary Table 1) for the subsurface layers.

Each grid-block in the surface soil layers was assigned a land use type (e.g. urban, paddy field) or land cover (e.g. forest) based on data published by the Ministry of the Environment (1986) and Ministry of Land, Infrastructure, Transport and Tourism (2006). The intrinsic permeability and effective porosity parameters for these grid-blocks are shown in Supplementary Table 2.

The soils within each grid-block of the surface soil layers were modeled with grain diameters of 0.001 mm, 0.01 mm, 0.1 mm, 0.3 mm, 1.0 mm, and 5.0 mm, respectively. We developed the grain size distribution for each type of land use and land cover (Supplementary Table 3) based on previous studies of basins in Japan (Mori et al., 2015).

Supplementary Fig. 1 shows how the relative permeability and the capillary pressure of the surface soil layers and subsurface grid blocks changes as a function of the water saturation within the grid block. Both these factors affect the flow of air and water underground in the model. The curves are based on van Genuchten's formulation (van Genuchten, 1980). The parameters in this model were fitted based on experimental data from the Japan Nuclear Cycle Development Institute (1999), Kinouchi and Watanabe (2011) and the Japan Institute of Construction Engineering (2012).

3. Simulation method and parameters

In order to simulate ^{137}Cs redistribution within surface water flows, subsurface fluid flows (air and water), we utilized the General-purpose Terrestrial fluid-Flow Simulator (GETFLOWS) code (Mori et al., 2014; 2015). Papers by Tosaka et al. (2000, 2010) and Mori et al. (2014; 2015) describe the details of GETFLOWS simulation code. The governing equations this code solves for fluid, sediment and radio-cesium transport are given in Mori et al. (2015).

The code models the effects of precipitation and evapo-transpiration on surface water flows (Harmon, 1961). The boundary conditions for the simulations were informed by meteorological data, including precipitation quantities measured by radar and at 8 weather stations over the periods simulated. During periods of heavy rain, we used radar AMeDAS data as precipitation inputs (JMA, 2011; 2013). Air temperature (5 stations), sunshine hours (5 stations), average wind velocity (5 stations) and relative humidity (3 stations) data were used to calculate evapo-transpiration. Manning's roughness coefficients, describing the resistance of the ground surface against surface water flows, are listed for each land use or vegetation type on the surface grid-blocks in Supplementary Table 4 (MLIT, 2014).

For sediment transport GETFLOWS simulates raindrop-induced soil detachment (Torri et al., 1987), including the effects of interception by forest canopies (Brandt, 1990), and direct erosion by surface water flows (Morgan et al., 1998; Kabir et al., 2011; Govers, 1990). Supplementary Table 5 lists model input parameters relating to rain-splash erosion, such as canopy height and coverage, broken down by land use and vegetation type. Supplementary Table 6 lists detachability indices for different soil types under rainfall impact and soil cohesive strengths affecting surface flow induced erosion.

The parameters chosen for our simulations (Supplementary Tables 1-6) were identical to those used in a previous GETFLOWS study of Fukushima basins (Kitamura et al., 2016). All parameters in Kitamura et al. (2016) were taken from literature values (Mori et al., 2015), with the exception of the soil detachability indices (Supplementary Table 6) and the parameters c and η affecting the transport capacity (TC) of sediment within surface water flows. These three parameters were tuned to correct a test simulation which overestimated the suspended sediment concentrations at low water flow rates at the Yaguno monitoring station on the Ukedo River. No further parameter tuning was undertaken for this study.

Radio-cesium is transported absorbed upon sediment particles or dissolved in water flows. The main input parameters concerning radio-cesium transport are shown in Table 2. Of particular importance is the initial inventory distribution in the study area, and the distribution coefficient, K_d, which describes the desorption of radio-cesium from soil particles into water. High K_d indicate low dissolution of radio-cesium from soil into water flows. We applied K_d value to sediment particles with grain diameter 0.3 mm and below. No radio-cesium was attached to grains over this size. Radio-cesium transport between soil layers occurs in the dissolved form by advection of groundwater, mechanical dispersion and molecular diffusion. Table 2 list the parameters for the mechanical dispersion and molecular diffusion components of the model.

Radio-cesium redistribution within the simulation periods were calculated as follows:

Step 1) Ten year average meteorological conditions are applied continuously until the equilibrium states of surface and sub-surface water flows are achieved.

Step 2) The sediment exchange layers of the model are introduced below the land surface, and water flow and sediment flows are simulated concurrently to equilibrate sediment flows using the same meteorological conditions as Step 1.

Step 3) Temporal rain conditions (e.g. typhoon conditions) are applied to the quasi-equilibrium states of water and sediment flow achieved by Step 2. The resulting water and sediment flows under flood conditions are simulated concurrently.

Step 4) Finally the radio-cesium distribution is initiated on the surface of the study area based on the Second Airborne Monitoring Survey (as shown in Fig. 1). Adsorption and desorption to sediments are simulated to trace the radio-cesium movement.

The simulation periods were Typhoon Roke in September 2011 and between January 2013 and December 2013. Nine heavy rainfall events occurred within this 2013 period, including four typhoons. The intensity of the different rainfall events can be seen in Fig. 3, which shows the total precipitation over the events broken down for each river basin.

4. Results and model validation

4.1 Surface and subsurface water flows

To validate the water flow component of the model we compared the simulation results for the water discharge rate with measurements taken at monitoring stations on the Odaka, Ukedo, Takase, Maeda, Kuma and Tomioka Rivers. The comparisons cover both periods of ambient flow conditions and during various rainfall events in 2013. Supplementary Fig. 2 shows the correlation of the predictions with the field measurements, from which we confirmed satisfactory performance of the water flow component of the model.

GETFLOWS calculates water flows on both the land surface and through the subsurface on the static 3D model of the basins. Information on watercourse locations are not provided *a priori* to the simulation code. Supplementary Fig. 3 shows streamlines of surface and subsurface water flows over the study area under ambient states of the river basins. The surface water flows propagate through the actual locations of river channels in the study area, showing the simulation is correctly calculating drainage patterns through the basins. It can also be seen that the subsurface water flows drain into the surface channels. Supplementary Fig. 4 show the subsurface water table contours, which correctly follow the land topography. Supplementary Fig. 5 shows the recharge and discharge fluxes of groundwater through the land surface in the study area. Between 2-4 mm/d of surface water drains to become groundwater across the study area to the west of the Futaba fault (Supplementary Fig. 5(a)). On the alluvial lowlands to the east of the Futaba fault, there is a relatively smaller recharge flux of 0-2 mm/d. The discharge of groundwater takes place mainly within the river channels (Supplementary Fig. 5(b)).

The results for the total water discharge from the Odaka, Ukedo, Maeda, Kuma and Tomioka rivers to the Pacific Ocean over 2011 Typhoon Roke and the nine rainfall events in 2013 are shown in Table 3. Also included are total ocean discharges for 2013, as well as the total water inflow to the Ogaki Dam Reservoir over the same periods. These results are shown graphically in Fig. 4.

4.2 Sediment flow during floods

Previously Kitamura et al. (2016) compared simulation and monitoring results for suspended sediment concentrations at two monitoring stations above the Ogaki Dam Reservoir. The simulations for both stations predicted the sediment concentration to good agreement with the observations during September 2013 flood events.

Table 4 and Fig. 5 show the total mass of sediment discharge to the ocean for the five main rivers over the different simulation periods. It also includes the result for sediment inflow to the Ogaki Dam. The locations where soil tends to be eroded and sediment depositions occur can be seen in Fig. 6, which shows the results of the Typhoon Roke simulation.

4.3 Radio-cesium migration

The main results of this study are reported in Table 5 and Fig. 7. These show the total ^{137}Cs discharge to the ocean via the five river mouth, and the ^{137}Cs inflow to the Ogaki Dam Reservoir, over the simulation periods. Figure 8 shows the net change in ^{137}Cs inventory occur Typhoon Roke across the study area. The general trend is that radio-cesium is eroded from the surface across much of the study area, thus lowering the inventory. Radio-cesium accumulates in specific locations within the basins, such as within dam reservoirs, along river beds and on flood plains within the river channels in the lower basins.

To validate the radio-cesium transport component of the simulation model, we compared simulation and monitoring results for radio-cesium concentrations (total of suspended and dissolved components) at the two monitoring stations (Hirusone and Yaguno) above the Ogaki Dam Reservoir (Fig. 9). The simulation results at both stations predict radio-cesium concentrations to good agreement with the observations obtained during two typhoons in 2013 (TRAAO, 2014).

We also compared the simulation results for ^{137}Cs discharge totals through monitoring stations on the Takase and Odaka rivers to measurements from 2013 (JAEA, 2014). For the Takase River, the total ^{137}Cs discharge through the monitoring station 2 km upstream from the river mouth over the first four rainfall events in 2013 was 30 GBq. The simulation result of 58 GBq through the same monitoring point is consistent with this. Similarly, 8 GBq of discharge past the monitoring station on the Odaka River 5 km upstream of the mouth was observed for January to November 2013, while the total simulation result for the major rainfall events during this period was 30 GBq. These simulation results fall within the uncertainty ranges of the observations.

5. Discussion

5.1 Trends of radio-cesium discharge to the ocean for different rainfall intensities

The radio-cesium discharge to the ocean in each event depends on the intensity of the rainfall. Figure 10 shows the correlation between total precipitation over each event and the amount of sediment and ^{137}Cs export to the Pacific Ocean from each river basin. In general, the higher the precipitation amount over the event, the larger the sediment and ^{137}Cs export.

Figure 10(b) shows clear differences between the amount of ^{137}Cs export to the ocean from the different basins for a given precipitation quantity. The cause of these differences between the basins are explored in the following section.

5.2 Transport of dissolved and solid phase radio-cesium

The relative importance of the dissolved and sediment-sorbed methods of radio-cesium transport depends on river flow rates. In the case of high water flow rates it is expected that the sediment-sorbed form would be the most important pathway. Fig. 11 shows simulation results for the dissolved and suspended ^{137}Cs concentrations as a function of river water flow at Hirusone monitoring station during 2013 Typhoon Wipha.

During the low flow rate period prior to Typhoon Wipha, the dissolved ^{137}Cs concentration is approximately 0.3 Bq/L. On the other hand, the suspended ^{137}Cs concentration is approximately 0.1 Bq/L. As the river flow rate increases during the flood, the ^{137}Cs concentration in the solid phase rises to a maximum of 90 Bq/L. The maximum in the dissolved phase is 0.6 Bq/L. Therefore, ^{137}Cs transport is mainly in the dissolved phase under ambient conditions, but dominated by the solid phase during flood events. This result is consistent with filed survey data, e.g. Nagao et al. (2013) and Ueda et al. (2013).

5.3 Characteristics of radio-cesium discharge between different basins

In absolute terms, the Ukedo River exports the highest inventory of ^{137}Cs to the ocean over each rainfall event (Fig. 7). This is mainly due to its catchment area, as it covers 63% of the study area (Table 1). However Fig. 10 shows substantial differences between the export of ^{137}Cs from the Odaka, Maeda, Kuma and Tomioka Rivers, despite the comparable catchment areas of these river basins. To investigate the factors controlling the differences in ^{137}Cs discharge between these basins, Fig. 12 plots the ratio of the ^{137}Cs discharge to the ocean over each rainfall event relative to the initial inventory within the basin at the Second Airborne Monitoring Survey (MEXT and MAFF, 2012).

The Maeda basin yields the largest ^{137}Cs discharge ratio for the majority of the events simulated. The total discharge for the 2013 rainfall events is 0.33% for this basin. This result compares with discharge ratios of 0.23%, 0.15%, 0.14% and 0.07% for the Kuma, Tomioka, Odaka and Ukedo river basins respectively. The magnitude of these discharge ratios are consistent with results from both modeling and monitoring of other fallout-contaminated basins within Fukushima Prefecture (Evrard et al., 2015).

The important factors which control the difference between these ratios are the initial distribution of radio-cesium within the basins (the fallout distribution), the susceptibility for sediment erosion to occur and be transported into channels, and the presence of dam reservoirs which act as sediments traps along the course of the rivers. The Maeda River has a high ^{137}Cs discharge ratio for the following reasons. The highest fallout contamination levels occur within the central part of the basin, which is downstream of the basin's dam reservoirs. The river is flanked by paddy fields as it runs through this contaminated area. Soil erosion and radio-cesium mobilization into rivers occurs more readily from paddy fields than from forests, thus resulting in a high ^{137}Cs discharge ratio.

The river with the second highest discharge ratio, the Kuma River, also shares these similarities with the Maeda basin. Its areas with highest fallout concentration lie in the central to lowland regions of the basin. This area is downstream of the Sakashita dam, which could trap contaminated sediments prior to export to the ocean. Paddy fields flank the Kuma River in its lowland areas.

The Maeda and Kuma basins contrast with the Ukedo River basin, which has the lowest discharge ratio. The highly contaminated areas of the Ukedo basin are the upstream areas covered in forests, where low export of radio-cesium occurs (Yoshimura et al. 2015a). The Ogaki Dam tends to trap highly contaminated sediments from its upstream areas migrating downstream of the dam.

The upstream Takase River mostly lies between the Hatagawa and Futaba faults. Here the fractured nature of the granite bedrock leads to high groundwater permeability (Kitamura et al., 2016). Figure 13 shows the degree of water saturation of the top surface soil layer over the course of the Typhoon Roke simulation. The area between the Hatagawa and Futaba faults maintains low saturation levels compared to the rest of the study area during the peak of the flood. This alleviates surface flooding levels, as precipitation is to an extent absorbed into groundwater, reducing surface flow derived soil erosion rates. The discharge of radio-cesium to the Takase River is reduced by this effect. For these reasons the Ukedo River has the lowest ^{137}Cs discharge ratio of the five main rivers in this study.

The discharge ratios for the Odaka and Tomioka Rivers are affected by the following factors. The area of the Odaka basin with the highest contamination lies in the uppermost forested part of the basin, also lying between the Hatagawa and Futaba faults. This causes a lower discharge ratio than the Maeda or Kuma Rivers. The Tomioka River has high contamination zones both in the central region and towards the coast. Migration of ^{137}Cs contaminated sediments downstream from the central region is limited by the Ogi and Takigawa dam reservoirs.

The results pertain to the importance of dam reservoir in limiting contaminated sediment migration downstream towards the ocean. Supplementary Table 7 summarizes the storage capacities and high water levels of the main dams in the study area.

5.4 Spatial distribution of sediment and ^{137}Cs erosion and deposition within the basins

The locations where the radio-cesium inventory tends to erode and to accumulate are important from a radiological and environmental perspective. Figures 6 and 8 respectively show the net change in sediment and radio-cesium inventory within the cells in the model over 2011 Typhoon Roke. Soil erosion occurs across the majority of the study area, as previously shown by Kitamura et al. (2016). The same pattern translates to radio-cesium as well. Net reductions in inventory occur across most of the cells covering the study area. The magnitude of the soil erosion is determined by hydrogeological features in the study area, while the absolute magnitude of reduction in radio-cesium inventory has a clear dependency on the initial fallout distribution as well (Fig. 8).

The reason for the correspondence between sediment and radio-cesium erosion patterns is due to the high K_d values in the Fukushima area (Yoshimura et al., 2015b). Radio-cesium is strongly sorbed to the sediment particles and the amount of dissolution into surface water flows is low. Therefore radio-cesium redistribution is primarily in the sediment-sorbed form.

Sediment deposition occurs on the flood plains within the river channels towards the eastern coastal area. Deposition also occurs on the beds of reservoirs, and curved or broad parts of rivers, and depressions on the land surface where surface water flow rates drop. These locations of sediment deposition are also locations for radio-cesium accumulation.

6. Conclusion

In this study, we have simulated water flows, sediment transport and radio-cesium migration under flooding conditions within five river basins near the FDNPP. Good agreement was obtained between the simulation results and monitoring data.

The simulations clarify the main locations of radio-cesium erosion, its flow paths through the study area, and the locations of accumulation over the flood events. Net reductions in the radio-cesium inventory occur across the majority of the land surface as a result of soil erosion. Some locations see net increases in the inventory due to sediment deposition. In particular these locations include certain flood plains adjacent to rivers, the beds of reservoirs, and curved or broad parts of rivers where the water flow rate drops.

In order to clarify the export of radio-cesium to the Pacific Ocean, we summarized the ^{137}Cs discharge and the discharge ratio from each river basin for various floods that occurred since 2011. The magnitude of ^{137}Cs discharge is affected by a number of factors. These include the size of the catchment, the density of ^{137}Cs fallout and its distribution within the catchment, the supply of ^{137}Cs to watercourses by erosion, and the presence of dam reservoirs along the watercourses.

We envisage that future studies will use the simulation results for water, sediment and radio-cesium movement through the basins for further research or to analyze remediation options. The results can be used as boundary conditions for more localized water channel and reservoir models, as well as Pacific Ocean transport models. Furthermore, the relationships between precipitation intensity and ^{137}Cs discharge could be used to predict amounts of sediment and ^{137}Cs discharge from the basins in future.

Acknowledgements

We acknowledge members of the Fukushima Environmental Safety Center and the Center for Computational Science & e-Systems for their contribution to the project, the Tohoku Regional Agricultural Administration Office for providing monitoring data, and the Geospatial Information Authority of Japan for providing land topography data created from the aerial laser survey. We also acknowledge K. Yoshimura, K. Iijima, K. Miyahara, and M. Yui for reviewing the manuscript, and Y. Onishi of Pacific Northwest National Laboratory for advising our modeling project.

Appendix A. Supplementary data

Supplementary data related to this article can be found in attached Word file to submission.

References

Abbott, M. B., Bathurst, J. C., Cunge, J. A., O'Connell, P. E., Rasmussen, J., 1986. An introduction to the European Hydrological System - Systeme Hydrologique Europeen, "SHE", 1: History and philosophy of a physically-based, distributed modelling system. J. Hydrol. 87, 45–59, DOI: 10.1016/0022-1694(86)90114-9.

Beven, K., 1989. Changing ideas in hydrology - The case of physically-based models. J. Hydrol. 105, 157–172, DOI: 10.1016/0022-1694(89)90101-7.

Brandt, C.J., 1990. Simulation of the size distribution and erosivity of raindrops and throughfall drops. Earth Surf. Process. Landf. 15, 687–698, DOI: 10.1002/esp.3290150803

Buesseler, K., 2014. Fukushima and ocean radioactivity. Oceanography 27, 92–105, DOI: 10.5670/oceanog.2014.02.

Chartin, C., Evrard, O., Onda, Y., Patin, J., Lefevre, I., Ottle, C., Ayrault, S., Lepage, H., Bonte, P., 2013. Tracking the early dispersion of contaminated sediment along rivers draining the Fukushima radioactive pollution plume. Anthropocene 1, 23–34, DOI: 10.1016/j.ancene.2013.07.001.

Evrard, O., Laceby, J.P., Lepage, H., Onda, Y., Cerdan, O., Ayrault, S., 2015. Radiocesium transfer from hillslopes to the Pacific Ocean after the Fukushima Nuclear Power Plant accident: A review. J. Environ. Radioact. 148, 92–110, DOI: 10.1016/j.jenvrad.2015.06.018.

Geological Survey of Japan, 2012. Seamless Digital Geological Map of Japan (1:200,000) https://gbank.gsj.jp/seamless/index_en.html (accessed 02.24.16).

Geospatial Information Authority of Japan, 2012. http://www.gsi.go.jp/ENGLISH/ (accessed 02.24.16)

Gonze, M.-A., Renaud, P., Korsakissok, I., Kato, H., Hinton, T.G., Mourlon, C., Simon-Cornu, M., 2014. Assessment of dry and wet atmospheric deposits of radioactive aerosols: Application to Fukushima radiocaesium fallout. Environ. Sci. Technol. 48, 11268–11276, DOI: 10.1021/es502590s.

Govers, G., 1990. Empirical relationships for transport capacity of overland flow, in *Erosion, transport and deposition processes* (Proceedings of the Jerusalem Workshop, March-April 1987), International Association of Hydrological Sciences, 189, 45–63.

Hamon, W.R., 1961. Estimating potential evapotranspiration, Proceedings American Society of Civil Engineers. 87(HY 3), 107-120.

IAEA, 2010. Handbook of parameter values for the prediction of radionuclide transfer in terrestrial and freshwater environments, Technical reports series. 472.

Japan Atomic Energy Agency (JAEA), 2014. Establishment of Technique for Identifying Long-term Impact of Radioactive Substances due to the Accident at the Fukushima Dai-ichi Nuclear Power Plant. http://fukushima.jaea.go.jp/initiatives/cat03/pdf06/2-4.pdf (accessed 09.04.15) (in Japanese).

Japan Institute of Construction Engineering, 2012. Guideline for structure investigation of river bank (in Japanese).

Japan Meteorological Agency (JMA), 2011 and 2013. Radar-AMeDAS data (in Japanese).

Japan Nuclear Cycle Development Institute, 1999. Technical confidence of the geological disposal for high-level nuclear waste in Japan. (in Japanese).

Kabir, M.A., Dutta1, D., Hironaka, S., 2011. Process-based distributed modeling approach for analysis of sediment dynamics in a river basin. Hydrol. Earth Syst. Sci. 15, 1307–1321, DOI: 10.5194/hess-15-1307-2011.

Katata, G., Ota, M., Terada, H., Chino, M., Nagai, H., 2012. Atmospheric discharge and dispersion of radionuclides during the Fukushima Dai-ichi Nuclear Power Plant accident. Part I: Source term estimation and local-scale atmospheric dispersion in early phase of the accident. J. Environ. Radioact. 109, 103–113, DOI: 10.1016/j.jenvrad.2012.02.006.

Kinouchi, T., Watanabe, Y., 2011. Hydrological model analysis considering spatial distribution of geological, soil and land use conditions. J. Japan Soc. Civil Eng., Ser. B1 (Hydraul. Eng.) 67, I_565–I_570, DOI: 10.2208/jscejhe.67.I_565.

Kinouchi T., Yoshimura K., Omata T. 2015. Modeling radiocesium transport from a river catchment based on a physically-based distributed hydrological and sediment erosion model. J. Environ. Radioact. 139**,** 407–415, DOI: 10.1016/j.jenvrad.2014.07.022.

Kitamura, A., Yamaguchi, H., Kurikami, Y., Yui, M., Onishi, Y., 2014. Predicting sediment and caesium-137 discharge from catchments in eastern Fukushima. Anthropocene 5, 22–31, DOI: 10.1016/j.ancene.2014.07.001.

Kitamura, A., Kurikami, H., Sakuma, K., Malins, A., Okumura, M., Machida, M., Mori, K., Tada, K., Tawara, Y., Kobayashi, T., Yoshida, T., Tosaka, H., 2016. Redistribution and export of contaminated sediment within eastern Fukushima Prefecture due to typhoon flooding. Earth Surf. Proc. Landforms (in press).

Koarashi, J., Atarashi-Andoh, M., Matsunaga, T., Sato, T., Nagao, S., Nagai, H., 2012. Factors affecting vertical distribution of Fukushima accident-derived radio- cesium in soil under different land-use conditions. Sci. Total Environ. 431, 392–401, DOI: 10.1016/j.scitotenv.2012.05.041.

Kobayashi, T., Nagai, H., Chino, M., Kawamura, H., 2013. Source term estimation of atmospheric release due to the Fukushima Dai-ichi Nuclear Power Plant accident by atmospheric and oceanic dispersion simulations. J. Nucl. Sci. Technol., 50, 255–264, DOI: 10.1080/00223131.2013.772449.

Matsuda, N., Mikami, S., Shimoura, S., Takahashi, J., Nakano, M., Shimada, K., Uno, K., Hagiwara, S., Saito, K., 2015. Depth profiles of radioactive cesium in soil using a scraper plate over a wide area surrounding the Fukushima Dai-ichi nuclear power plant, Japan. J. Environ. Radioact. 139, 427-434. DOI: 10.1016/j.jenvrad.2014.10.001.

Matsunaga, T., Koarashi, J., Atarashi-Andoh, M., Nagao, S., Sato, T., Nagai, H., 2013. Comparison of the vertical distributions of Fukushima nuclear accident radio- cesium in soil before and after the first rainy season, with physicochemical and mineralogical interpretations. Sci. Total Environ. 447, 301–314, DOI: 10.1016/j.scitotenv.2012.12.087.

MEXT and MAFF, 2012. Ministry of Education, Culture, Sports, Science and Technology (MEXT), and Ministry of Agriculture, Forestry and Fisheries (MAFF). Summarized Version of the "Results of the Research on Distribution of Radioactive substances Discharged by the Accident at TEPCO's Fukushima Dai-ichi NPP". http://radioactivity.nsr.go.jp/en/contents/1000/294/24/PressR04%200802s.pdf (accessed 09.04.15).

Ministry of the Environment (MOE), 1986. National Surveys on the Natural Environment. http://www.biodic.go.jp/kiso/fnd_f.html (accessed 09.04.15).

Ministry of Land, Infrastructure, Transport and Tourism (MLIT), 2006.

http://nlftp.mlit.go.jp/ksj/jpgis/datalist/KsjTmplt-L03-b.html (accessed 09.04.15).

Ministry of Land, Infrastructure, Transport and Tourism (MLIT), 2014. http://www.mlit.go.jp/river/shishin_guideline/gijutsu/gijutsukijunn/index2.html (accessed 02.25.16)

Monteith, J.L., 1981. Evaporation and surface temperature. Quart. J. Roy. Meteorolog. Soc., 107, 1–27, DOI: 10.1002/qj.49710745102.

Morgan, R.P.C., Quinton, J.N., Smith, R.E., Govers, G., Poesen, J.W.A., Auerswald, K., Chisci, G., Torri, D., Styczen, M.E., 1998. The European soil erosion model (EUROSEM): a dynamic approach for predicting sediment transport from fields and small catchments. Earth Surf. Process. Landf. 23, 27–544, DOI: 10.1002/(SICI)1096-9837(199806).

Mori, K., Tada, K., Tawara, Y., Ohno, K., Asami, M., Kosaka, K., Tosaka, H., 2014. An integrated watershed modeling to assess the long-term fate of Fukushima derived radionuclides. International Environmental Modelling and Software Society (iEMSs) 7th International Congress on Environmental Modelling and Software, San Diego, CA.

Mori, K., Tada, K., Tawara, Y., Ohno, K., Asami, M., Kosaka, K., Tosaka, H., 2015. Integrated watershed modeling for simulation of spatiotemporal redistribution of post-fallout radionuclides: Application in radiocesium fate and transport processes derived from the Fukushima accidents. Environ. Model. Softw. 72, 126–146, DOI: 10.1016/j.envsoft.2015.06.012.

Nagao, S., Kanamori, M., Ochiai, S., Tomihara, S., Fukushi, K., Yamamoto, M., 2013. Export of ^{134}Cs and ^{137}Cs in the Fukushima river systems at heavy rains by typhoon Roke in September 2011. Biogeosciences 10, 6215-6223. DOI: 10.5194/bg-10-6215-2013.

Nakanishi T., Matsunaga T., Koarashi J., Atarashi-Andoh M., 2014. ^{137}Cs vertical migration in a deciduous forest soil following the Fukushima Dai-ichi Nuclear Power Plant accident. J. Environ. Radioact. 128, 9–14, DOI: 10.1016/j.jenvrad.2013.10.019.

Onishi, Y., Voitsekhovich, O.V., Zheleznyak, M.J., 2007. Chernobyl – What Have We Learned?, Springer, ISBN: 978-1-4020-5348-1.

Saegusa, H., Ohyama, T., Iijima, K., Onoe, H., Takeuchi, R., Hagiwara, H., 2016. Deposition of radiocesium on the river flood plains around Fukushima, J. Environ. Radioact. 164, 36–46, DOI: 10.1016/j.jenvrad.2016.04.020.

Saito T., Makino H., Tanaka S., 2014. Geochemical and grain-size distribution of radioactive and stable cesium in Fukushima soils: implications for their long-term behavior. J. Environ. Radioact. 138, 11–18, DOI: 10.1016/j.jenvrad.2014.07.025.

Takahashi, J., Tamura, K., Suda, T., Matsumura, R., Onda, Y., 2015. Vertical distribution and temporal changes of 137Cs in soil profiles under various land uses after the Fukushima Dai-ichi Nuclear Power Plant accident, J. Environ. Radioact. 139, 351–361, DOI: 10.1016/j.jenvrad.2014.07.004.

Terada, H., Katata, G., Chino, M., Nagai, H., 2012. Atmospheric discharge and dispersion of radionuclides during the Fukushima Dai-ichi Nuclear Power Plant accident. Part II: Verification of the source term and analysis of regional-scale atmospheric dispersion. J. Environ. Radioact. 112, 141–154, DOI: 10.1016/j.jenvrad.2012.05.023.

Teramage, M.T., Onda, Y., Patin, J., Kato, H., Gomi, T., Nam, S., 2014. Vertical distribution of radiocesium in coniferous forest soil after the Fukushima Nuclear Power Plant accident. J. Environ. Radioact. 137, 37–45, DOI: 10.1016/j.jenvrad.2014.06.017.

Tohoku Regional Agricultural Administration Office (TRAAO), 2014. http://www.maff.go.jp/tohoku/osirase/higai_taisaku/hukkou/140918_torimatome.html (in Japanese) (accessed 9 March 2015).

Torri, D., Sfalaga, M., Del Sette, M., 1987. Splash detachment: runoff depth and soil cohesion. Catena 14, 149–155, DOI: 10.1016/S0341-8162(87)80013-9.

Tosaka, H., Itho, K., Furuno, T., 2000. Fully coupled formulation of surface flow with 2-phase subsurface flow for hydrological simulation. Hydrol. Process. 14, 449–464, DOI: 10.1002/(SICI)1099-1085(20000228).

Tosaka, H., Mori, K., Tada, K., Tawara, Y., Yamashita, K., 2010. A general-purpose terrestrial fluids/heat flow simulator for watershed system management. IAHR International Groundwater Symposium 2010, Valancia, Spain.

Ueda, S., Hasegawa, H., Kakiuchi, H., Akata, N., Ohtsuka, Y., Hisamatsu, S., 2013. Fluvial discharges of radiocaesium from watersheds contaminated by the Fukushima Dai-ichi Nuclear Power Plant accident, Japan. J. Environ. Radioact. 118, 96-104. DOI: 10.1016/j.jenvrad.2012.11.009.

van Genuchten, M.Th. (1980), A closed-form equation for predicting the hydraulic conductivity of unsaturated soils. Soil Sci. Soc. Am. J. 44, 892–898, DOI: 10.2136/sssaj1980.03615995004400050002x.

Yamaguchi, M., Kitamura, A., Oda, Y., Onishi, Y., 2014. Predicting the long-term ^{137}Cs distribution in Fukushima after the Fukushima Dai-ichi nuclear power plant accident: a parameter sensitivity analysis. J. Environ. Radioact. 135, 135–146, DOI: 10.1016/j.jenvrad.2014.04.011.

Yoshimura, K., Onda, Y., Fukushima, T., 2014. Sediment particle size and initial radiocesium accumulation in ponds following the Fukushima DNPP accident. Sci. Rep. 4, 4514, DOI: 10.1038/srep04514.

Yoshimura K., Onda Y., Kato H. 2015a. Evaluation of radiocaesium wash-off by soil erosion from various land uses using USLE plots. J. Environ. Radioact. 139, 362–369, DOI: 10.1016/j.jenvrad.2014.07.019.

Yoshimura K., Onda Y., Sakaguchi A., Yamamoto M., Matsuura Y. 2015b. An extensive study of the concentrations of particulate/dissolved radiocaesium derived from the Fukushima Dai-ichi Nuclear Power Plant accident in various river systems and their relationship with catchment inventory. J. Environ. Radioact. 139, 370–378, DOI: 10.1016/j.jenvrad.2014.08.021.

Table 1 Characteristics of each basin.

	Catchment area	Forest	Rice paddy	Crop field	Building	Other	Max. elevation in basin (a)	Distance from river source to mouth (b)	Average slope (a)/(b)	Initial inventory (^{137}Cs)
(Unit)	km^2	%	%	%	%	%	m	km	m/m	TBq
Odaka	67.7	49	26	14	7	4	380	15	0.0253	47.92
Ukedo	423.6	57	25	7	5	6	550	35	0.0157	832.74
Maeda	45.5	75	8	10	2	5	259	14	0.0185	71.5
Kuma	74.8	71	14	5	6	4	551	18	0.0306	86.41
Tomioka	62.1	71	13	5	6	5	500	17	0.0294	38.49
Total	673.7	60	22	7	5	5	-	-	-	1077.06

Table 2 Radio-cesium transport parameters

	Unit	Notes
Half-life	y	30.1
Inventory	Bq/m^2	Second Airborne Monitoring Survey [a]
Distribution coefficient K_d	L/kg	400,000 [b]
Molecular diffusion coefficient	m^2/s	2.07×10^{-9} (in water at 25 ℃)
Tortuosity factor	-	0.5
Longitudinal and transverse dispersion lengths	m	0.1 (Longitudinal), 0.01 (Transverse)
Representative length	m	1

a MEXT and MAFF (2012) – excludes 5 km zone surrounding Fukushima Daiichi Nuclear Site

b IAEA (2010) – for sediment grains up to 0.3 mm, no radio-cesium absorbed to larger grains

Table 3 Amount of water discharge to the ocean over nine heavy rainfall events in 2013, as well as Typhoon Roke in September 2011. Final column shows water inflow to the Ogaki Dam Reservoir in the Ukedo basin over the rainfall events.

	Total water discharge to ocean (m^3)					Total water inflow to dam (m^3)
period	Odaka Riv.	Ukedo Riv.	Maeda Riv.	Kuma Riv.	Tomioka Riv.	Ogaki Dam
2-4 Apr. 2013	1.57E+06	5.78E+06	1.56E+06	2.02E+06	1.60E+06	9.04E+05
14-16 June 2013	1.66E+06	3.88E+06	9.55E+05	1.01E+06	4.71E+05	7.46E+05
26-28 July 2013	1.09E+06	7.70E+06	8.97E+05	1.56E+06	1.38E+06	2.22E+06
5-7 Aug. 2013	7.30E+05	7.95E+06	1.22E+06	1.23E+06	1.27E+06	2.14E+06
14-16 Sep. 2013	2.50E+06	1.53E+07	1.64E+06	2.40E+06	2.15E+06	3.52E+06
1-3 Oct. 2013	1.05E+06	4.26E+06	9.03E+05	1.24E+06	1.13E+06	9.60E+05
15-17 Oct. 2013	4.91E+06	2.11E+07	3.81E+06	4.60E+06	4.16E+06	3.98E+06
19-21 Oct. 2013	3.46E+06	1.45E+07	2.90E+06	3.90E+06	3.60E+06	2.77E+06
22-24 Oct. 2013	2.03E+06	9.18E+06	1.27E+06	1.90E+06	1.80E+06	2.08E+06
Total 2013 events	1.90E+07	8.96E+07	1.52E+07	1.99E+07	1.76E+07	1.93E+07
20-22 Sep. 2011	8.20E+06	4.90E+07	6.84E+06	9.40E+06	8.59E+06	9.32E+06

Table 4 Amount of sediment discharge to the ocean over nine heavy rainfall events in 2013, as well as Typhoon Roke in September 2011. Final column shows sediment inflow to the Ogaki Dam Reservoir in the Ukedo basin over the rainfall events.

	Total sediment discharge to ocean (kg)					Total sediment inflow to dam (kg)
period	Odaka Riv.	Ukedo Riv.	Maeda Riv.	Kuma Riv.	Tomioka Riv.	Ogaki Dam
2-4 Apr. 2013	2.36E+05	4.97E+05	3.46E+05	2.13E+05	1.39E+05	3.81E+04
14-16 June 2013	7.02E+05	4.83E+05	2.45E+05	1.32E+05	2.20E+04	7.08E+04
26-28 July 2013	1.08E+05	2.50E+05	7.32E+04	1.09E+05	1.25E+05	9.21E+04
5-7 Aug. 2013	3.33E+04	4.05E+05	3.02E+05	6.59E+04	6.59E+04	6.09E+04
14-16 Sep. 2013	7.79E+05	2.95E+06	4.19E+05	3.04E+05	1.85E+05	7.60E+05
1-3 Oct. 2013	1.11E+05	1.57E+05	8.45E+04	8.41E+04	6.72E+04	8.88E+03
15-17 Oct. 2013	1.48E+06	4.57E+06	1.37E+06	7.74E+05	5.89E+05	7.86E+05
19-21 Oct. 2013	7.79E+05	2.95E+06	4.19E+05	3.04E+05	1.85E+05	7.60E+05
22-24 Oct. 2013	3.28E+05	3.21E+05	1.66E+05	1.01E+05	7.47E+04	3.28E+04
Total 2013 events	4.56E+06	1.26E+07	3.42E+06	2.09E+06	1.45E+06	2.61E+06
20-22 Sep. 2011	1.80E+06	8.80E+06	1.65E+06	1.97E+06	1.70E+06	2.09E+06

Table 5 Amount of ^{137}Cs discharge to the ocean over nine heavy rainfall events in 2013, as well as Typhoon Roke in September 2011. Final column shows ^{137}Cs inflow to the Ogaki Dam Reservoir in the Ukedo basin over the rainfall events.

	Total ^{137}Cs discharge to ocean (GBq)					Total ^{137}Cs inflow to dam (GBq)
period	Odaka Riv.	Ukedo Riv.	Maeda Riv.	Kuma Riv.	Tomioka Riv.	Ogaki Dam
2-4 Apr. 2013	2.6	30.0	16.6	14.8	4.2	6.5
14-16 June 2013	13.0	26.1	7.7	8.8	0.7	10.5
26-28 July 2013	1.3	13.1	3.7	8.2	4.7	16.0
5-7 Aug. 2013	0.3	15.4	7.5	4.4	2.6	11.1
14-16 Sep. 2013	12.3	144.0	22.6	19.6	6.0	146.9
1-3 Oct. 2013	0.9	8.2	2.4	5.9	2.4	1.8
15-17 Oct. 2013	21.8	218.0	91.2	61.4	17.5	146.2
19-21 Oct. 2013	14.7	78.8	76.2	72.4	19.2	32.6
22-24 Oct. 2013	2.3	20.1	5.9	7.0	2.1	8.1
Total 2013 events	69.3	553.7	233.8	202.6	59.5	379.6
20-22 Sep. 2011	29.2	502.6	116.5	106.0	25.0	333.1

Figure captions

Fig. 1 The five river basins in the study area. The shading shows the initial ^{137}Cs distribution on the surface based on the Second Airborne Monitoring Survey (MEXT and MAFF, 2012). ^{137}Cs inventory data was not gathered within the 5 km zone surrounding the Fukushima Daiichi site during the Second Airborne Survey, and therefore the radio-cesium redistribution results of this study do not cover this area.

Fig. 2 Bird's-eye view of the three dimensional grid block system developed for the study area.

Fig. 3 Precipitation within each river basin over the periods of the different rainfall events.

Fig. 4 Total water discharge from the Odaka, Ukedo, Maeda, Kuma and Tomioka rivers to the Pacific Ocean over September 2011 Typhoon Roke and the 2013 rainfall events. Also included are orange bars showing total water inflow to the Ogaki Dam over each period.

Fig. 5 Total sediment discharge from the five rivers to the Pacific Ocean over Typhoon Roke and the 2013 rainfall events, as well as inflow to the Ogaki Dam.

Fig. 6 Locations of sediment erosion/deposition across the study area over 2011 Typhoon Roke.

Fig. 7 Total ^{137}Cs discharge from the Odaka, Ukedo, Maeda, Kuma and Tomioka rivers to the Pacific Ocean over Typhoon Roke and the 2013 events, as well total inflow to the Ogaki Dam reservoir.

Fig. 8 The net change in ^{137}Cs inventory over Typhoon Roke across the study area.

Fig. 9 Simulation predictions and monitoring results for radio-cesium concentrations (total of dissolved and sediment-sorbed components) at the Hirusone and Yaguno monitoring on the upstream Ukedo River. Squares show discontinuous monitoring results taken year round. Circles show continuous monitoring data measured especially over typhoon periods.

Fig. 10 (a) Relationship between water and sediment discharge to the ocean, and (b) that of water and ^{137}Cs discharge, for the nine rainfall events in 2013.

Fig. 11 Dissolved and suspended ^{137}Cs concentration as a function of river water flow at Hirusone monitoring station during 2013 Typhoon Wipha.

Fig. 12 The ratio of ^{137}Cs activity discharged to the ocean to the total inventory of the basin at the Second Airborne Monitoring Survey over each of the flood events. The results for the Ogaki Dam show the ratio of ^{137}Cs activity inflow to the reservoir relative to the initial inventory upstream of the reservoir at the Second Monitoring Survey.

Fig. 13 Distribution of water saturation in the top surface soil layer before, during, and after 2011 Typhoon Roke.

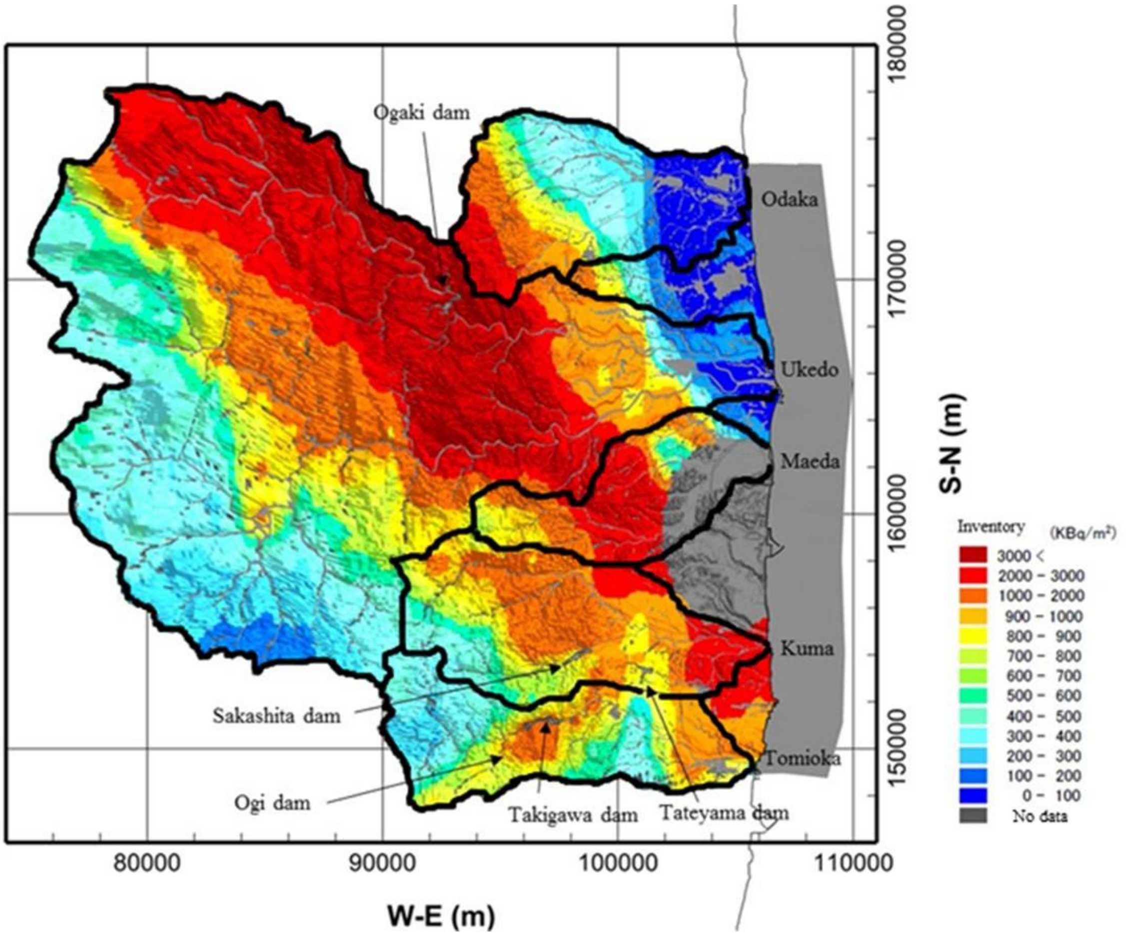
Ogaki dam
Odaka
Ukedo
Maeda
Kuma
Tomioka
Sakashita dam
Ogi dam
Takigawa dam
Tateyama dam
80000
90000
100000
110000
W-E (m)
150000
160000
170000
180000
S-N (m)
Inventory (KBq/m²)
3000 <
2000 - 3000
1000 - 2000
900 - 1000
800 - 900
700 - 800
600 - 700
500 - 600
400 - 500
300 - 400
200 - 300
100 - 200
0 - 100
No data

Fig. 1

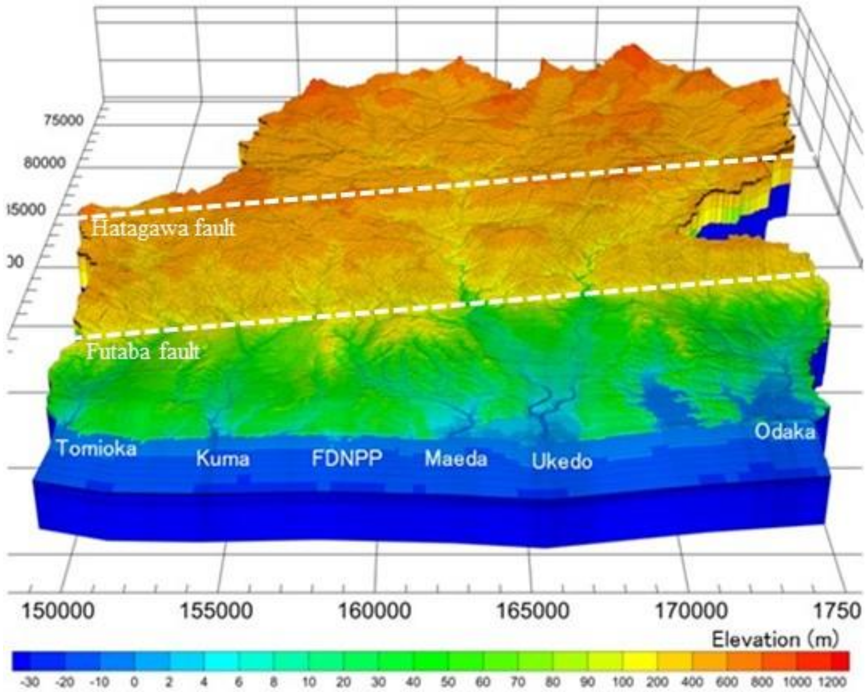
75000
80000
Hatagawa fault
Futaba fault
Tomioka
Kuma
FDNPP
Maeda
Ukedo
Odaka
150000
155000
160000
165000
170000
Elevation (m)
-30 -20 -10 0 2 4 6 8 10 20 30 40 50 60 70 80 90 100 200 400 600 800 1000 1200

Fig. 2

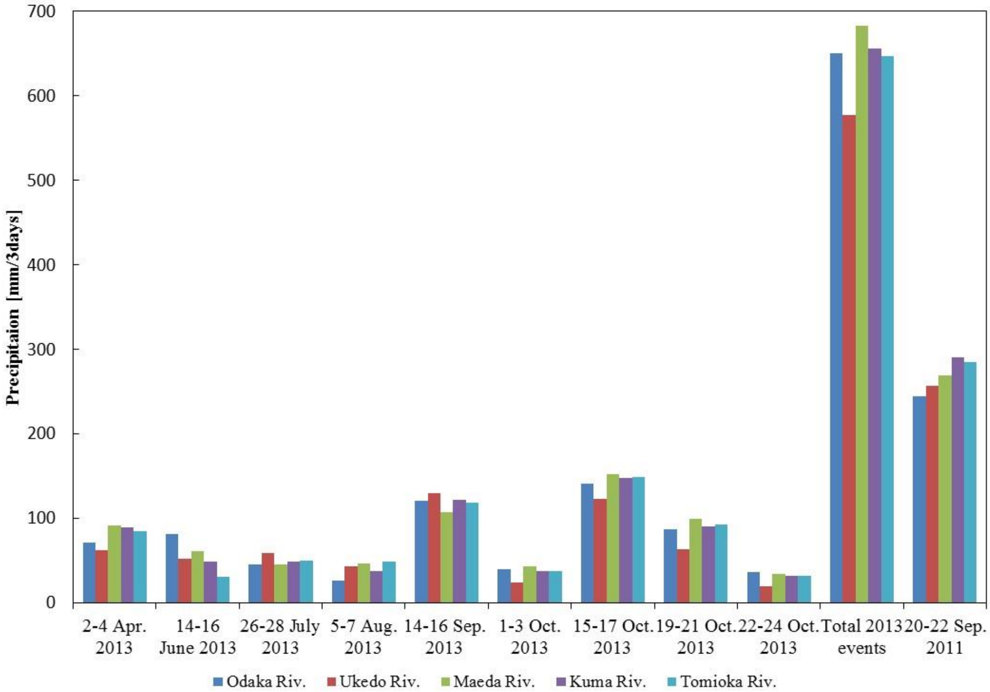

Fig. 3

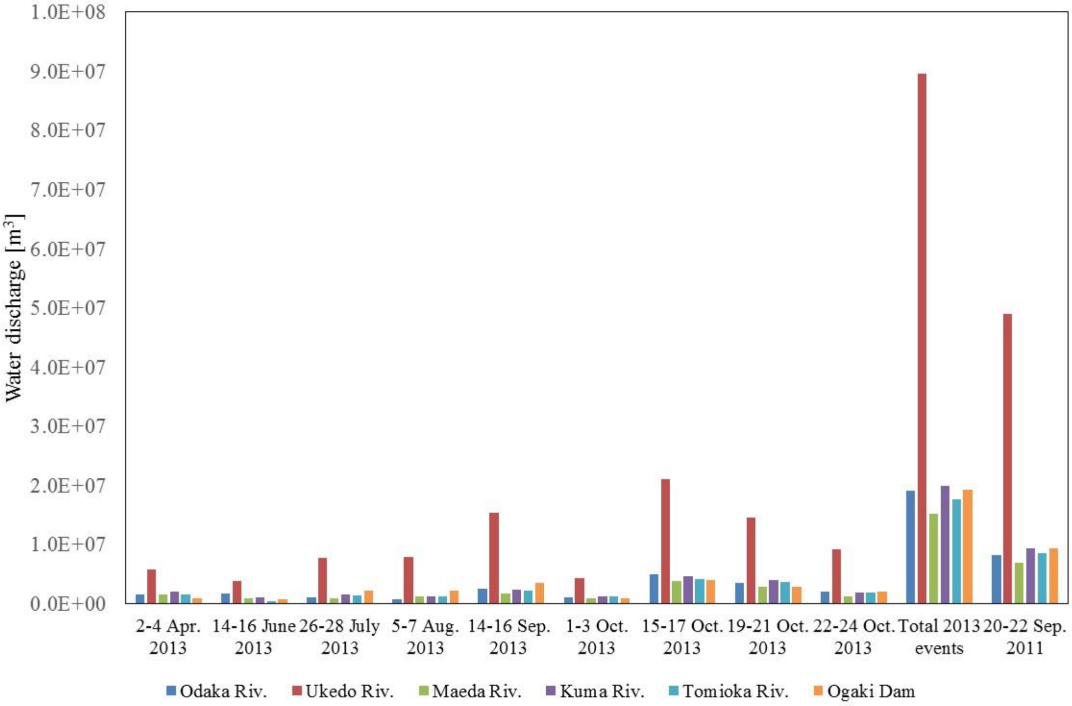

Fig. 4

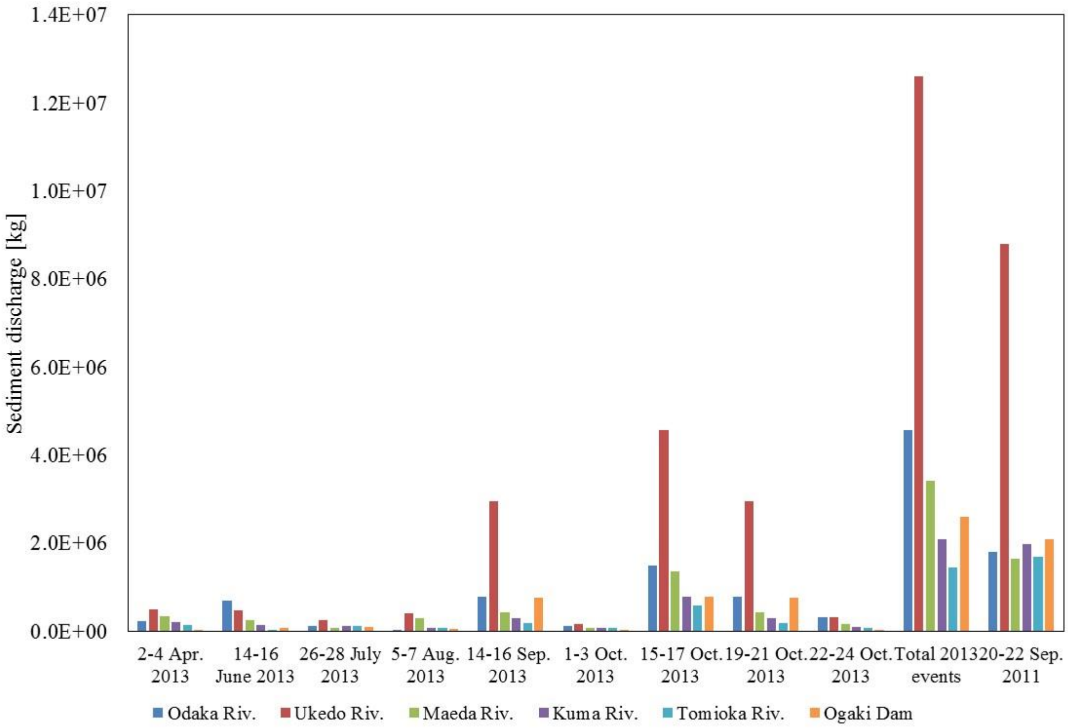

Sediment discharge [kg]
1.4E+07
1.2E+07
1.0E+07
8.0E+06
6.0E+06
4.0E+06
2.0E+06
0.0E+00
2-4 Apr. 2013
14-16 June 2013
26-28 July 2013
5-7 Aug. 2013
14-16 Sep. 2013
1-3 Oct. 2013
15-17 Oct. 2013
19-21 Oct. 2013
22-24 Oct. 2013
Total 2013 events
20-22 Sep. 2011
Odaka Riv.
Ukedo Riv.
Maeda Riv.
Kuma Riv.
Tomioka Riv.
Ogaki Dam

Fig. 5

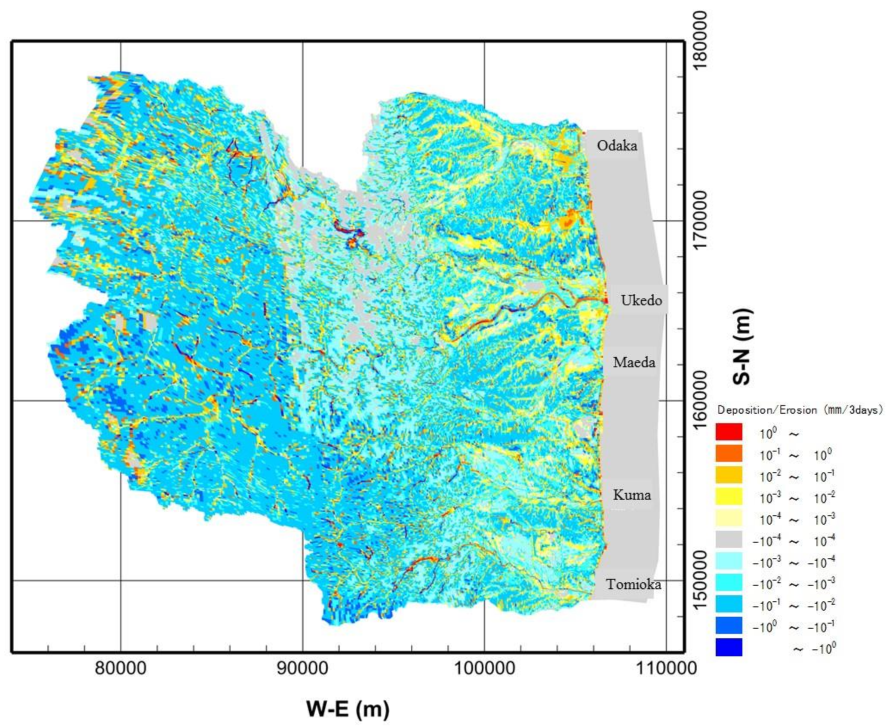

Odaka
Ukedo
Maeda
Kuma
Tomioka
S-N (m)
180000
170000
160000
150000
W-E (m)
80000
90000
100000
110000
Deposition/Erosion (mm/3days)

Fig. 6

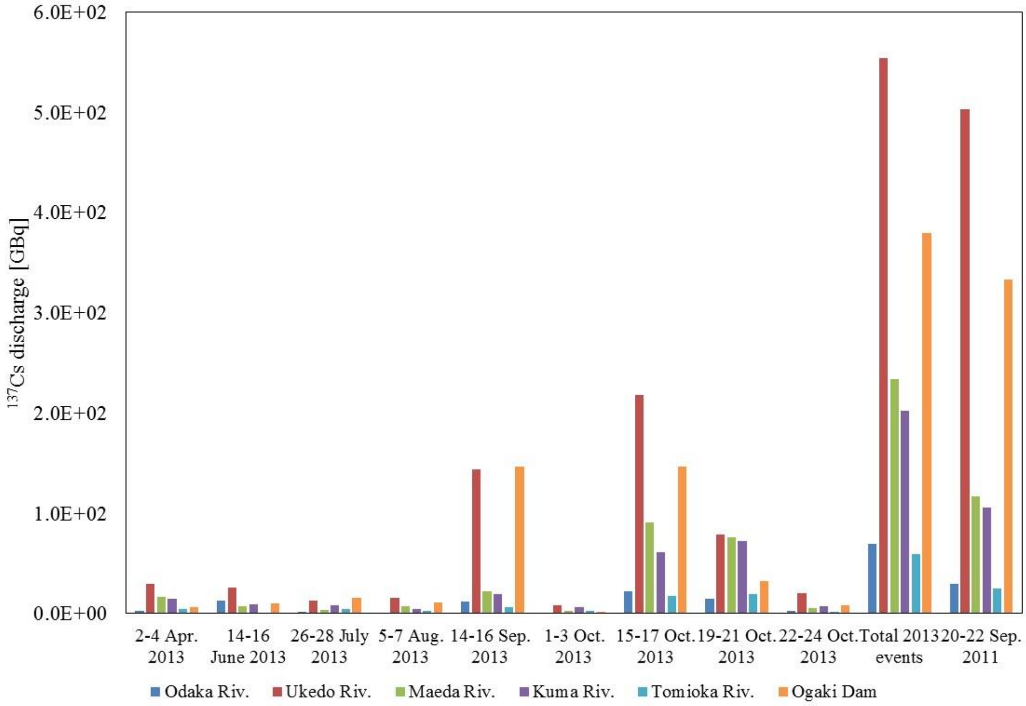

6.0E+02
5.0E+02
4.0E+02
3.0E+02
2.0E+02
1.0E+02
0.0E+00
137Cs discharge [GBq]
2-4 Apr. 2013
14-16 June 2013
26-28 July 2013
5-7 Aug. 2013
14-16 Sep. 2013
1-3 Oct. 2013
15-17 Oct. 2013
19-21 Oct. 2013
22-24 Oct. 2013
Total 2013 events
20-22 Sep. 2011
Odaka Riv.
Ukedo Riv.
Maeda Riv.
Kuma Riv.
Tomioka Riv.
Ogaki Dam

Fig. 7

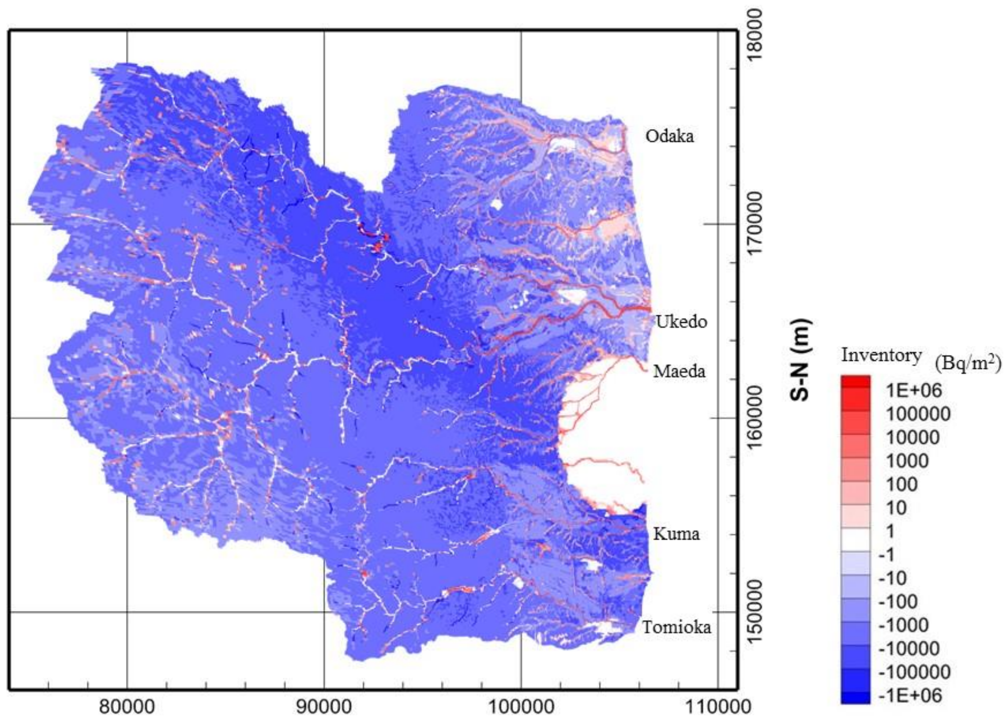

Odaka
Ukedo
Maeda
Kuma
Tomioka
80000
90000
100000
110000
150000
160000
170000
180000
S-N (m)
Inventory (Bq/m2)
1E+06
100000
10000
1000
100
10
1
-1
-10
-100
-1000
-10000
-100000
-1E+06

Fig. 8

Hirusone

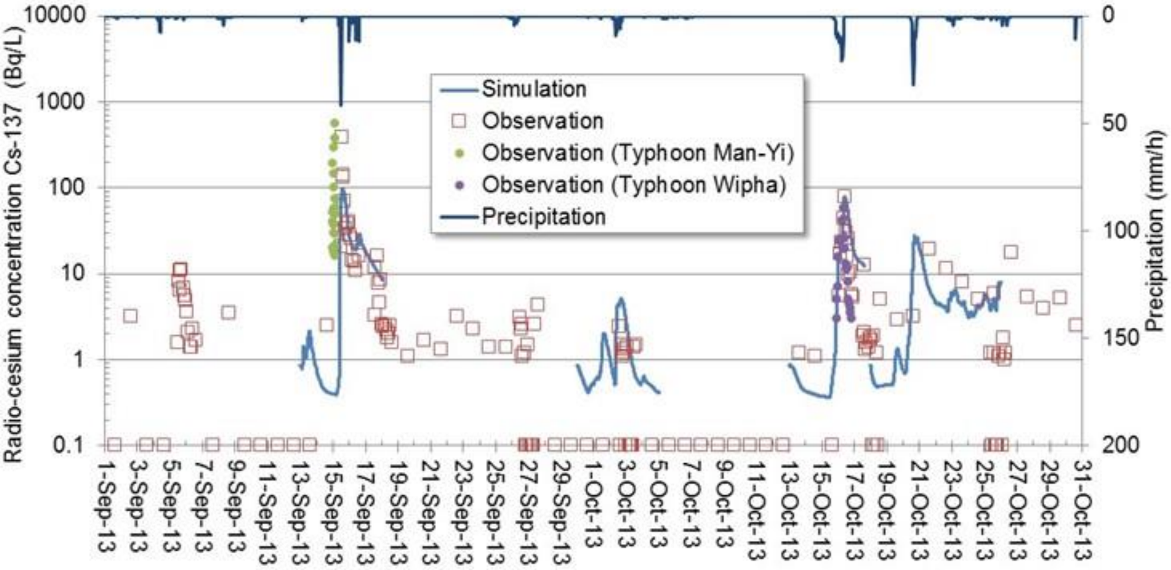

Yaguno

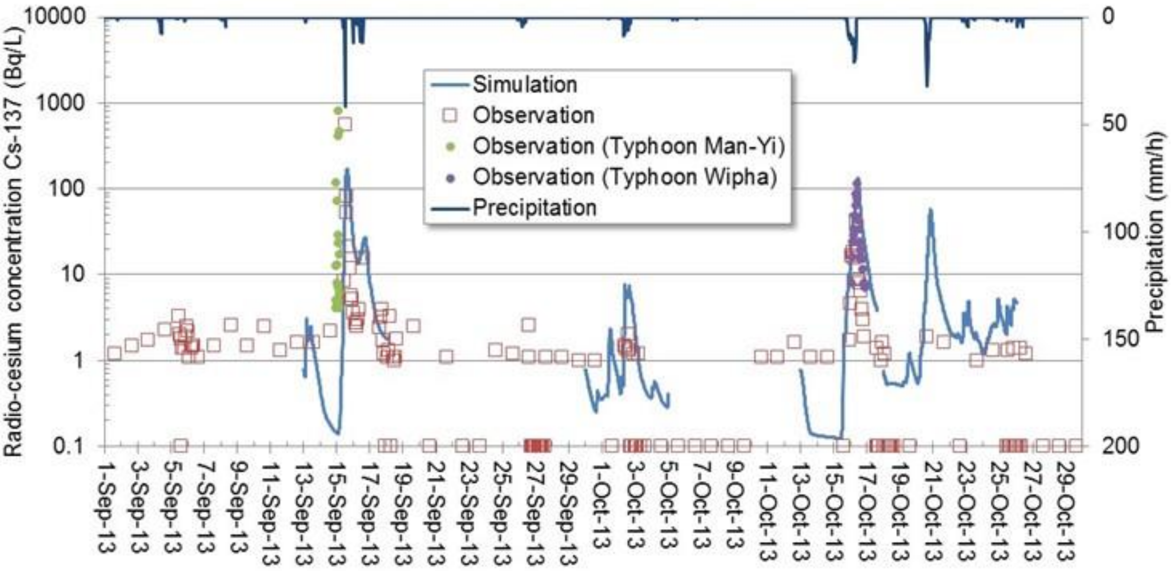

Fig. 9

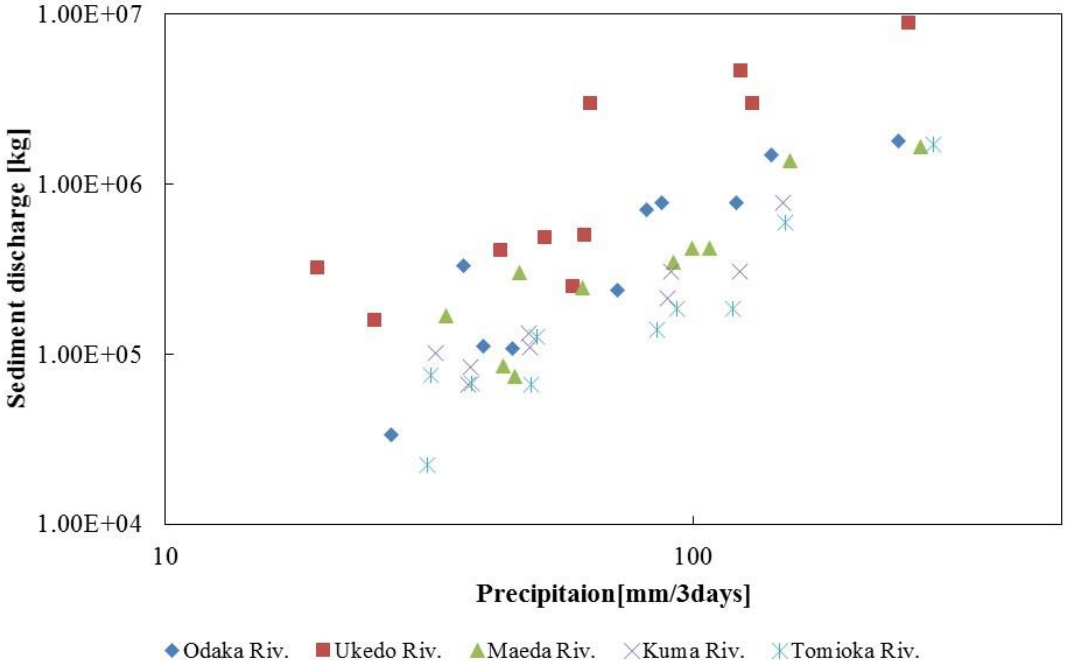
1.00E+07
1.00E+06
1.00E+05
1.00E+04
Sediment discharge [kg]
10
100
Precipitaion[mm/3days]
Odaka Riv.
Ukedo Riv.
Maeda Riv.
Kuma Riv.
Tomioka Riv.

(a)

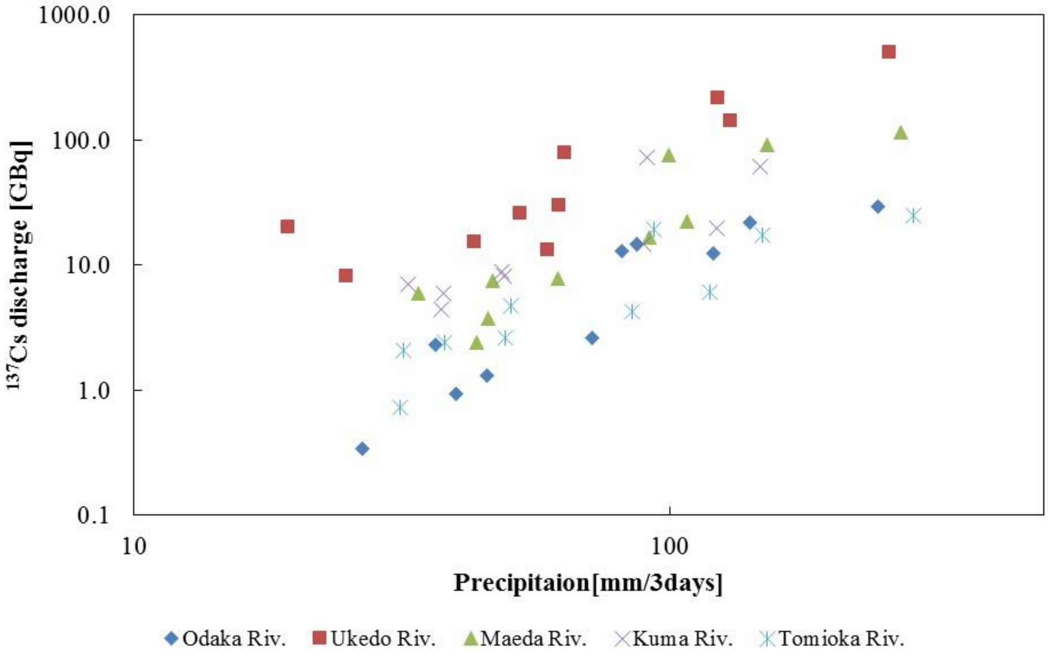
1000.0
100.0
10.0
1.0
0.1
^{137}Cs discharge [GBq]
10
100
Precipitaion[mm/3days]
Odaka Riv.
Ukedo Riv.
Maeda Riv.
Kuma Riv.
Tomioka Riv.

(b)

Fig. 10

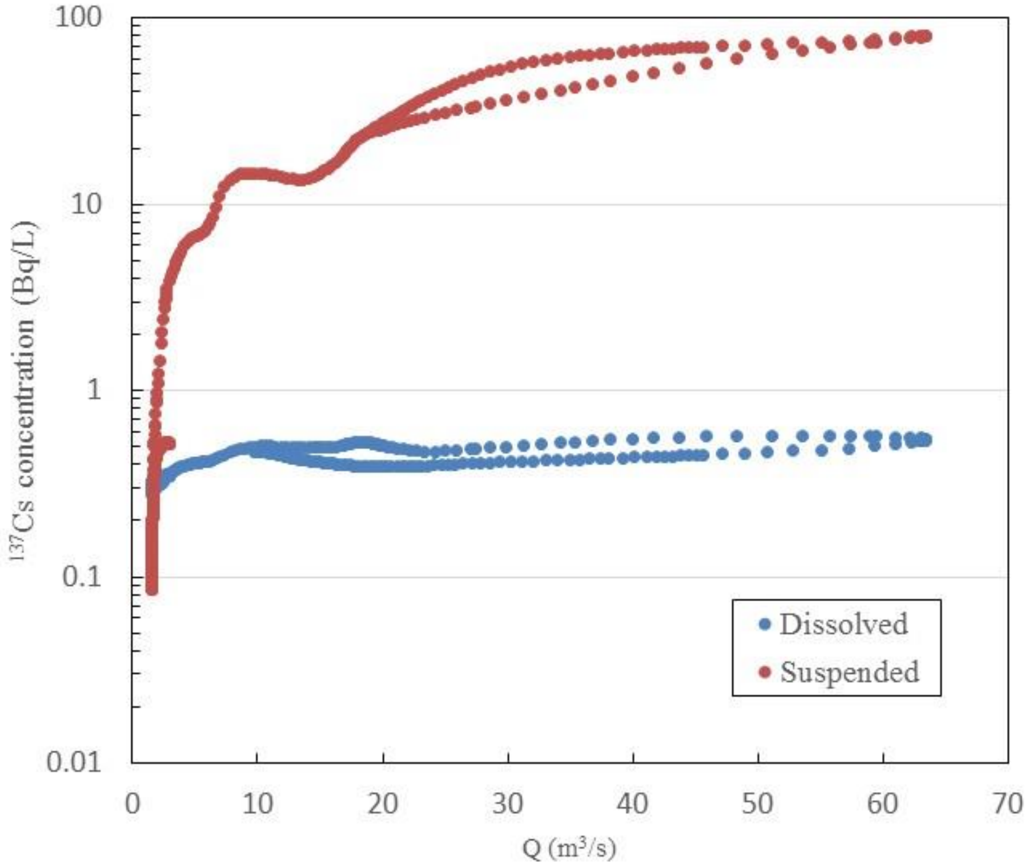

100
10
1
0.1
0.01
0
10
20
30
40
50
60
70
^{137}Cs concentration (Bq/L)
Q (m^3/s)
Dissolved
Suspended

Fig. 11

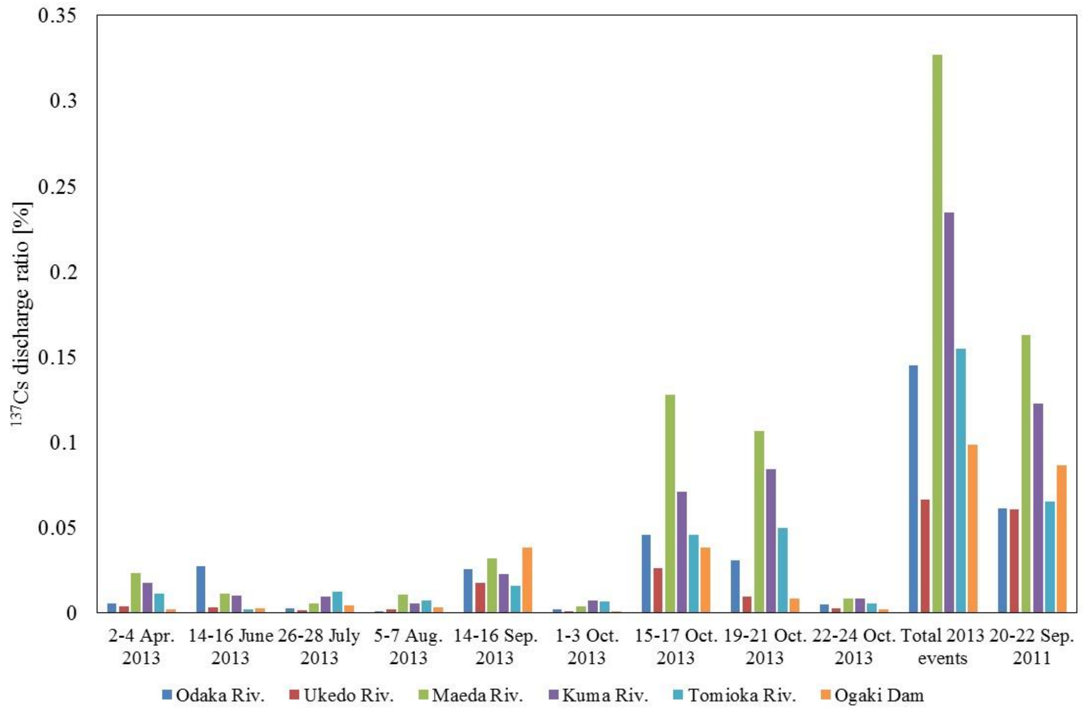

0.35
0.3
0.25
0.2
0.15
0.1
0.05
0
^{137}Cs discharge ratio [%]
2-4 Apr. 2013
14-16 June 2013
26-28 July 2013
5-7 Aug. 2013
14-16 Sep. 2013
1-3 Oct. 2013
15-17 Oct. 2013
19-21 Oct. 2013
22-24 Oct. 2013
Total 2013 events
20-22 Sep. 2011
Odaka Riv.
Ukedo Riv.
Maeda Riv.
Kuma Riv.
Tomioka Riv.
Ogaki Dam

Fig. 12

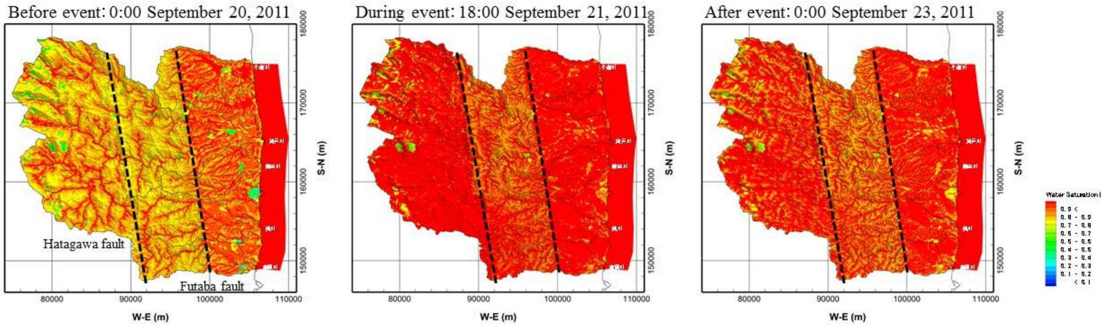
Before event: 0:00 September 20, 2011
During event: 18:00 September 21, 2011
After event: 0:00 September 23, 2011
Hatagawa fault
Futaba fault
W-E (m)
S-N (m)
80000
90000
100000
110000
150000
160000
170000
180000

Fig. 13

Characteristics of radio-cesium transport and discharge between different basins near to the Fukushima Dai-ichi Nuclear Power Plant after heavy rainfall events

Kazuyuki Sakuma, Akihiro Kitamura, Alex Malins, Hiroshi Kurikami, Masahiko Machida, Koji Mori, Kazuhiro Tada, Takamaru Kobayashi, Yasuhiro Tawara, Hiroyuki Tosaka.

Supplementary material

Supplementary Fig. 1 Relative permeability curve and capillary pressure curves for surface soil and subsurface grid blocks.

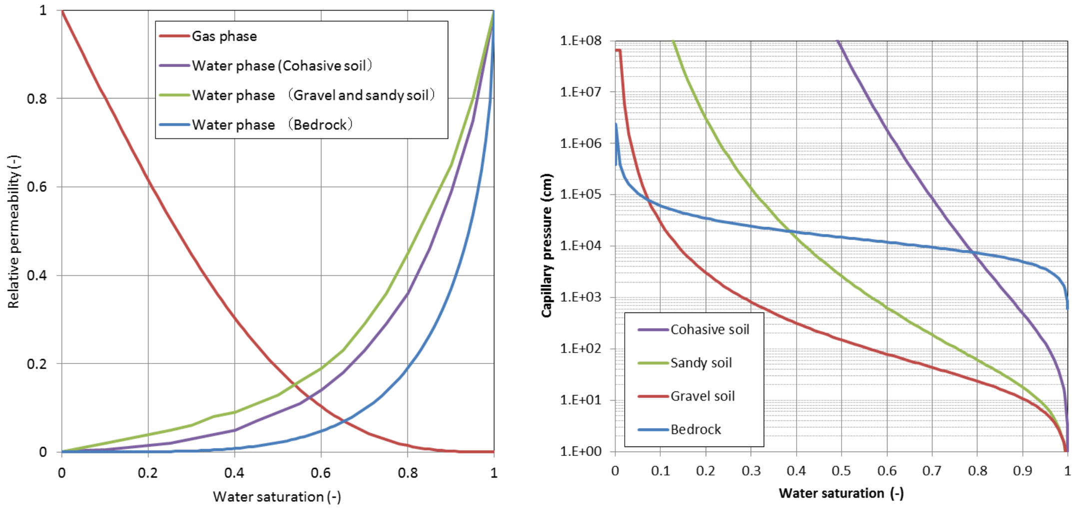

Supplementary Fig. 2 Comparison of simulated with observed water discharge rates at monitoring stations on the Odaka, Ukedo, Takase, Maeda, Kuma and Tomioka Rivers. Superimposed on each panel is the Pearson correlation coefficient (r).

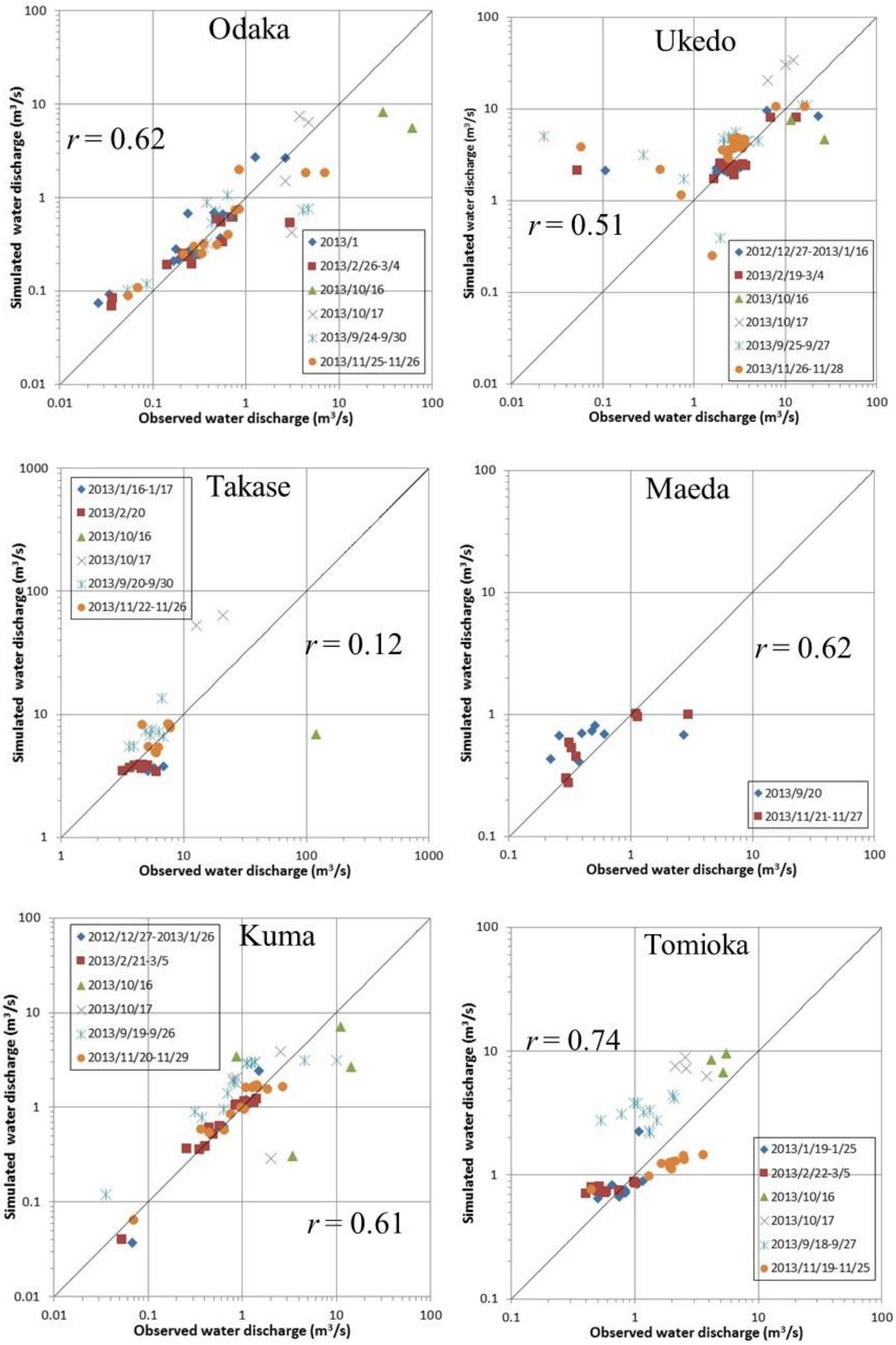

Supplementary Fig. 3 Streamlines of surface water flow and subsurface flow of the study area under ambient flow conditions.

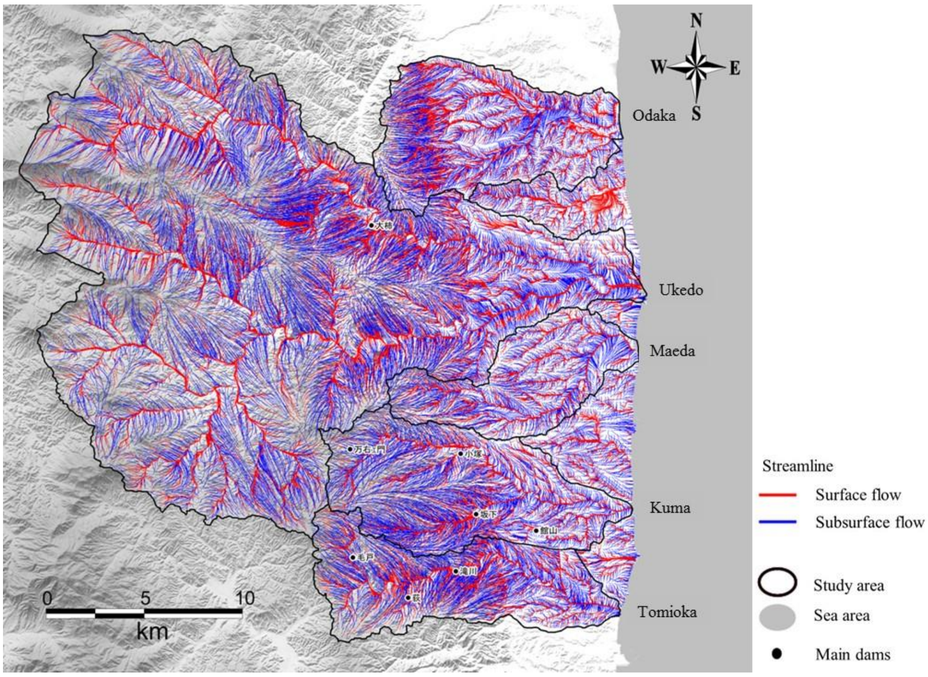

Supplementary Fig. 4 Subsurface water table contours under ambient conditions

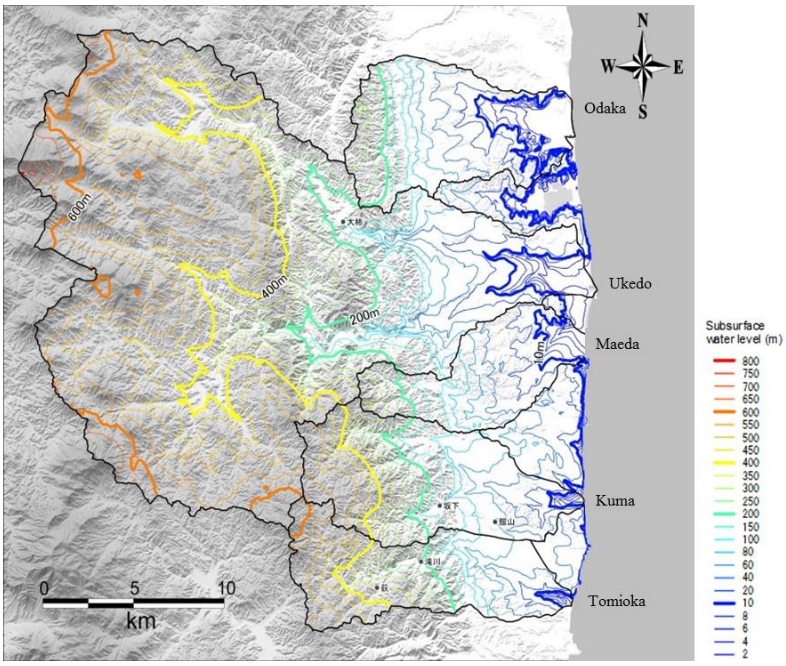

Supplementary Fig. 5 (a) Recharge flux and (b) discharge flux of groundwater through the land surface in the study area under ambient conditions.

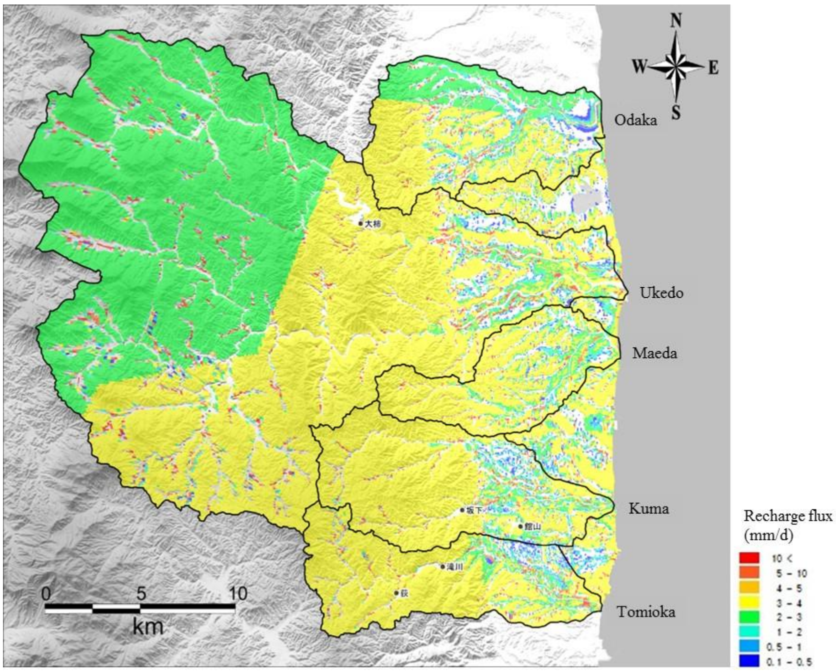

(a)

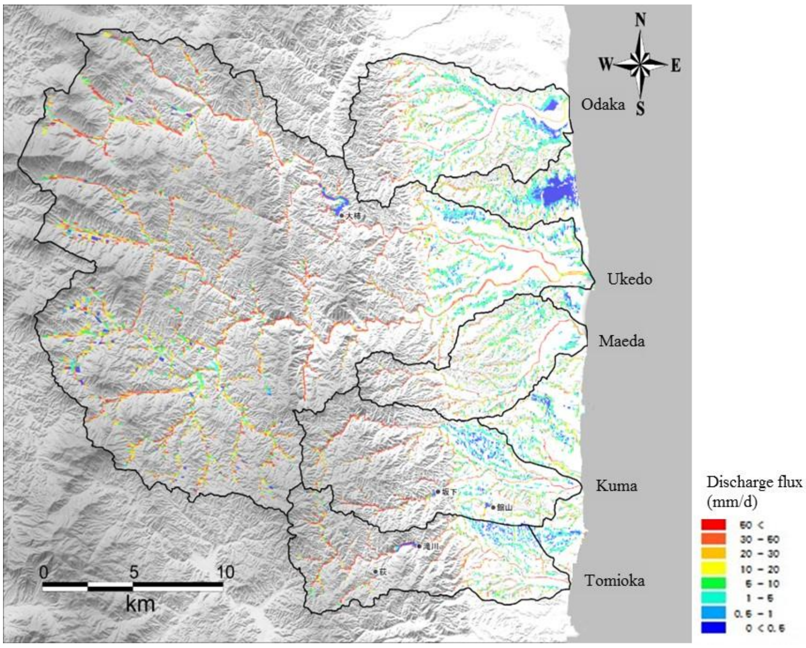

(b)

Supplementary Table 1 Hydraulic parameters for grid-blocks in the subsurface layers

Classification	Subdivision	Intrinsic permeability (m/s)	Effective porosity (-)
Deposits in mountainous area	Riverbed gravel	1×10^{-4}	0.3
	Hillside deposit	3×10^{-5}	0.3
	Landslide soil mass	3×10^{-5}	0.3
Alluvium	Sand-rich	H*:1×10^{-4} V*:1×10^{-5}	0.3
	Clay-rich	H:1×10^{-6} V:1×10^{-7}	0.2
Terrace deposits	Lower, Middle, Marine, Higher	3×10^{-5}	0.3
Dainenji formation	Upper alternate layer	H:1×10^{-5} V:1.1×10^{-8}	0.3
	Middle mudstone	1.1×10^{-8}	0.2
	Lower mudstone	H:1×10^{-6} V:1×10^{-7}	0.3
Basement rocks	Weathered (western area)	H:5×10^{-7} V:1×10^{-8}	0.2
	Weathered (eastern area)	1×10^{-6}	0.2
	Fresh	1×10^{-8}	0.1

*H: horizontal, V: vertical

Supplementary Table 2 Hydraulic parameters for grid-blocks in the surface soil layer

Land use and land cover	Subsurface	Intrinsic permeability (m/s)	Effective porosity (-)	Relative permeability curve and capillary curve
Urban city		5×10^{-7}	0.25	Sandy soil
Compound		5×10^{-5}	0.3	Gravel soil
Paddy		1×10^{-7}	0.2	Cohesive soil
Mountains and forests, waste land, farmland	Deposit on slope surface	1×10^{-3}	0.5	Gravel soil
	Alluvium with gravel			
	Alluvium with sand			
	Alluvium with clay			Cohesive soil
	Terrace (Lower, Marine, mid, high)			
	Dainenji formation (Upper, Middle, Lower)			
	Weathered host rock			
Sand dune plant	Alluvium with sand			Gravel soil
Glay soil, glay lowland soil, andosol on farmland				Gravel soil
Glay soil, glay lowland soil		1×10^{-7}	0.2	Cohesive soil
Andosol		1×10^{-3}	0.5	Cohesive soil
Peat bed ~ muck soil		1×10^{-5}	0.7	Cohesive soil

Supplementary Table 3 Sediment particle size distribution

Land use and land cover	Subsurface		Sediment particle size					
			0.001 mm	0.01 mm	0.1 mm	0.3 mm	1.0 mm	5.0 mm
Urban city			-	-	-	-	-	-
Compound			(Categorized by mountains in forest, waste land, farmland)					
Paddy			0.2	0.6	0.1	0.05	0.05	-
Mountains and forests, waste land, farmland	Deposit on slope surface		0.05	0.3	0.1	0.1	0.15	0.3
	Alluvium with gravel		0.05	0.15	0.1	0.1	0.2	0.4
	Alluvium with sand		0.05	0.15	0.3	0.3	0.2	-
	Alluvium with clay		0.2	0.7	0.1	-	-	-
	Terrace	Lower	0.05	0.2	0.15	0.2	0.1	0.3
		Marine, mid, high	0.1	0.6	0.1	0.1	0.1	-
	Dainenji formation	Upper	0.1	0.6	0.1	0.1	0.1	-
		Middle	0.2	0.7	0.1	-	-	-
		Lower	0.05	0.55	0.2	0.1	0.1	-
	Weathered host rock		0.05	0.4	0.15	0.2	0.1	0.1
Sand dune plant	Alluvium with sand		-	0.3	0.5	0.2	-	-
Glay soil, glay lowland soil, andosol on farmland			0.2	0.5	0.2	0.05	0.05	-
Glay soil, glay lowland soil			0.2	0.5	0.2	0.05	0.05	-
Andosol			0.1	0.4	0.2	0.2	0.1	-
Peat bed ~ muck soil			0.2	0.6	0.2	-	-	-

T. Saito et al., 2014

T. Nakanishi et al., 2014

M.T. Teramage et al., 2014

J. Takahashi et al., 2015

J. Koarashi et al., 2012

Supplementary Table 4 Manning's roughness coefficient for each land use and vegetation

Land use and vegetation	Manning's roughness coefficient ($m^{-1/3}$ s)
Urban area and industrial sites	0.1
Compounds with grass	0.2
Grassland	0.3
Paddy (fallow fields)	0.2
Farmland (abandoned)	0.4
Orchards and mulberry fields	0.4
Land with weeds (Miscanthus sinensis)	0.5
Waterside grassland (Phraqmites australis)	0.05
Dune vegetation	0.3
Cutover area	0.5
Conifer forest	0.5
Japanese cedar and Japanese cypress	0.5
Larch	0.5
Broad leaved deciduous trees	0.8
River	0.03
Reservoir	0.01

Supplementary Table 5 Raindrop-induced erosion parameters

Land use and vegetation	Height (m)	Stem storage (mm)	Crown covering (-)	Floor storage (mm)	Floor covering (-)
Urban areas and industrial sites	0	0.5	0	0	0
Compounds with grass	0.5	0.5	0	0	0
Grassland	0.3	0.5	0.9	0	0
Paddy (fallow fields)	0	0.5	0.9	0	0
Farmland (abandoned)	0.3	0.5	0.9	0	0
Orchards and mulberry fields	3	0.5	0.5	0.25	0.5
Land with weeds (Miscanthus sinensis)	0.5	0.5	0.9	0	0
Waterside grassland (Phraqmites australis)	0.05	0.5	0.9	0	0
Dune vegetation	0.3	0.5	0.8	0	0
Cutover area	0.5	0.5	0.9	0	0
Conifer forest	15	1.5	0.8	0.25	0.95
Japanese cedar and Japanese cypress	15	1.5	0.8	0.25	0.95
Larch	15	1.5	0.8	0.25	0.95
Broad leaved deciduous trees	15	1	0.8	0.25	0.95
River	0	0	0	0	0
Reservoir	0	0	0	0	0

Supplementary Table 6 Soil detachment properties

Land use land cover	Subsurface	Soil Detachability Index (g/J)	Cohesive strength (kPa)
Urban city		-	0
Compound		(Categorized by mountains in forest, waste land, farmland)	
Paddy		2.4	10
Mountains and forests, waste land, farmland	Deposit on slope surface	3	3
	Alluvium with gravel		
	Alluvium with sand		
	Alluvium with clay	2.4	10
	Terrace (Lower, Marine, mid, high)		
	Dainenji formation (Upper, Middle, Lower)		
	Weathered host rock		
Sand dune plant	Alluvium with sand	6	2
Glay soil, glay lowland soil, andosol on farmland		2.4	10
Glay soil, glay lowland soil			
Andosol			
Peat bed ~ muck soil			

Supplementary Table 7 Main dam reservoirs in the study area

Dam reservoir	River	Volume ($1000\ m^3$)	Max water height (T.P. m)
Ogaki	Ukedo	17300	170
Ogi	Oginosawa	716	357.5*
Sakashita	Ohkawahara	2532	127*
Takigawa	Tomioka	5165	215
Tateyama	Tomioka	1286	60*

Data published by association of the dam in japan.

*Calculated value from digital elevation map data of Japan (Geospatial Information Authority of Japan, 2012)